bioRxiv preprint doi: https://doi.org/10.1101/2020.07.06.190181; this version posted July 6, 2020. The copyright holder for this preprint (which was not certified by peer review) is the author/funder. All rights reserved. No reuse allowed without permission.

Title: High-throughput cultivation of stable, diverse, fecal-derived microbial communities to model the intestinal microbiota

Authors: Andrés Aranda-Díaz[1], Katharine Michelle Ng[1], Tani Thomsen[1], Imperio Real-Ramírez[1], Dylan Dahan[2], Susannah Dittmar[1], Carlos Gutierrez Gonzalez[3], Taylor Chavez[1], Kimberly S. Vasquez[2], Taylor H. Nguyen[1], Feiqiao Brian Yu[4], Steven K. Higginbottom[2], Norma F. Neff[4], Joshua E. Elias[4], Justin L. Sonnenburg[2,4], Kerwyn Casey Huang[2,4*]

[1]Department of Bioengineering, Stanford University, Stanford, CA 94305

[2]Department of Microbiology and Immunology, Stanford University School of Medicine, Stanford, CA 94305

[3]Department of Chemical and Systems Biology, Stanford University School of Medicine, Stanford, CA 94305

[4]Chan Zuckerberg Biohub, San Francisco, CA 94158

[*]Correspondence: kchuang@stanford.edu

Lead author: Kerwyn Casey Huang, kchuang@stanford.edu

bioRxiv preprint doi: https://doi.org/10.1101/2020.07.06.190181; this version posted July 6, 2020. The copyright holder for this preprint (which was not certified by peer review) is the author/funder. All rights reserved. No reuse allowed without permission.

Keywords: *gut microbiota; ciprofloxacin; antibiotics; microbial ecology; culturomics; ex vivo; synthetic communities; microbiota perturbations; ecological stability*

bioRxiv preprint doi: https://doi.org/10.1101/2020.07.06.190181; this version posted July 6, 2020. The copyright holder for this preprint (which was not certified by peer review) is the author/funder. All rights reserved. No reuse allowed without permission.

Summary

Mechanistic understanding of the impacts of the gut microbiota on human health has been hampered by limited throughput in animal models. To enable systematic interrogation of gut-relevant microbial communities, here we generated hundreds of *in vitro* communities cultured from diverse stool samples in various media. Species composition revealed stool-derived communities that are phylogenetically complex, diverse, stable, and highly reproducible. Community membership depended on both medium and initial inoculum, with certain media preserving inoculum compositions. Different inocula yielded different community compositions, indicating their potential for personalized therapeutics. Communities were robust to freezing and large-volume culturing, enabling future translational applications. Defined communities were generated from isolates and reconstituted growth and composition similar to those of communities derived from stool inocula. Finally, *in vitro* experiments probing the response to ciprofloxacin successfully predicted many changes observed *in vivo*, including the resilience and sensitivity of each *Bacteroides* species. Thus, stool-derived *in vitro* communities constitute a powerful resource for microbiota research.

bioRxiv preprint doi: https://doi.org/10.1101/2020.07.06.190181; this version posted July 6, 2020. The copyright holder for this preprint (which was not certified by peer review) is the author/funder. All rights reserved. No reuse allowed without permission.

Introduction

The gut microbiota is a diverse community that performs functions important for host physiology, including interactions with the immune system (Hooper et al., 2012), metabolism (Sonnenburg and Backhed, 2016), and the nervous system (Mayer et al., 2014). A wide range of environmental perturbations, including diet (Kashyap et al., 2013), antibiotics (Schubert et al., 2015), and osmotic diarrhea (Tropini et al., 2018), lead to changes in community composition and function. Human and animal models have enabled some mechanistic understanding of these responses. For example, gnotobiotic mouse models provide insights into particular microbial communities (Becker et al., 2011; Faith et al., 2011; Mark Welch et al., 2017; Reyes et al., 2013; Rezzonico et al., 2011; Turnbaugh et al., 2009) composed of a single species, a defined set of species, or of complex samples originating from specific hosts such as humans.

Importantly, our understanding of microbiota recovery from antibiotics is limited. Antibiotics disrupt colonization resistance and lead to pathogen expansion and fecal shedding (Barthel et al., 2003; Doorduyn et al., 2006; Lawley et al., 2008; Pavia et al., 1990; Stecher et al., 2007), and can affect host physiology, including changes in adiposity, insulin resistance, and cognitive function (Cho et al., 2012; Cox et al., 2014; Frohlich et al., 2016; Hwang et al., 2015). Understanding antibiotic effects across microbiotas, doses, and treatment regimens will assist in mitigating these adverse

bioRxiv preprint doi: https://doi.org/10.1101/2020.07.06.190181; this version posted July 6, 2020. The copyright holder for this preprint (which was not certified by peer review) is the author/funder. All rights reserved. No reuse allowed without permission.

effects. We recently showed, using mice colonized with human feces, that the microbiota shifts into a new, lower-diversity steady state after ciprofloxacin treatment, although certain taxa displayed a high level of resilience during recovery (Ng et al., 2019). It is unclear to what extent the response of each taxon can be predicted from its behavior in isolation; microbial interactions and drug modification can impact the efficacy of antibiotic treatment (Adamowicz et al., 2018; de Vos et al., 2017; Nicoloff and Andersson, 2016; Sanchez-Vizuete et al., 2015), which may underlie our current inability to explain individualized responses to fluoroquinolone treatment in humans (Dethlefsen and Relman, 2011) or to understand why some antibiotics, like vancomycin, negatively impact taxa known to be resistant to the drug *in vitro* (Ivanov et al., 2008).

In vivo investigations of the gut microbiota of humans and mice are limited in throughput, and it is often difficult to isolate and quantitatively tune the magnitude of perturbations. As a complementary approach, synthetic *in vitro* co-culturing of a defined community of isolated species has revealed key interspecies interactions and metabolic roles (de Vos et al., 2017; Gutierrez and Garrido, 2019; Kehe et al., 2019; Venturelli et al., 2018). However, such bottom-up approaches generally lack the complexity of typical gut microbiotas; further, microbes coexisting in a host shape each other's evolutionary paths (Barroso-Batista et al., 2020), which could underlie individualized responses of the human gut microbiota to antibiotics (Dethlefsen and

bioRxiv preprint doi: https://doi.org/10.1101/2020.07.06.190181; this version posted July 6, 2020. The copyright holder for this preprint (which was not certified by peer review) is the author/funder. All rights reserved. No reuse allowed without permission.

Relman, 2011). It is difficult to select a particular set of species to model complex ecosystems such as the mammalian gut without *a priori* knowledge of interspecies interactions; most approaches therefore choose representative species from the major taxa.

While sophisticated continuous-flow culture models (Macfarlane et al., 1998; Minekus et al., 1999; Van de Wiele et al., 2015) permit long time-scale experimentation and the manipulation of key environmental variables, these systems are also limited in throughput (to date, mini-bioreactor arrays have included 48 reactors running in parallel; (Auchtung et al., 2016). Other approaches to study the function of complex microbiotas *in vitro* include *ex vivo* resuspensions of stool or other natural communities in liquid media, for example to analyze drug metabolism by highly complex communities (Zimmermann et al., 2019). These approaches are higher throughput, but the extent to which they recapitulate the gut environment is not clear, and they have yet to be used to systematically study community assembly and growth from gut samples. In a recent study, diverse microbiomes from leaf and soil samples were passaged in minimal media with a single carbon source (Goldford et al., 2018). Batch culturing led to the selection of simple communities whose compositions were predictably governed by nutrient availability at the family but not the species level, revealing alternative species-

bioRxiv preprint doi: https://doi.org/10.1101/2020.07.06.190181; this version posted July 6, 2020. The copyright holder for this preprint (which was not certified by peer review) is the author/funder. All rights reserved. No reuse allowed without permission.

level community assembly patterns (Goldford et al., 2018). The extent to which these findings extend to human-relevant microbiotas and more complex media is unknown.

To close these gaps, here we established that top-down, stool-derived *in vitro* communities (SICs) are powerful tools for modeling responses of the gut microbiota to perturbations *in vivo*. We demonstrated that hundreds of SICs generated from distinct initial inocula in diverse media can be phylogenetically complex and diverse, and preserve the structure of the initial inoculum with generally stable and reproducible compositions. SICs can be frozen, grown in larger volumes, and reconstituted from isolates without affecting composition. Most importantly, upon antibiotic treatment, many of the responses of the SICs mimicked changes observed in the antibiotic-treated humanized gnotobiotic mice from which the initial inocula were sampled, indicating that SICs could be used to predict and interpret the results of *in vivo* experiments in high throughput.

bioRxiv preprint doi: https://doi.org/10.1101/2020.07.06.190181; this version posted July 6, 2020. The copyright holder for this preprint (which was not certified by peer review) is the author/funder. All rights reserved. No reuse allowed without permission.

Results

Diet and antibiotic treatment provide a diverse pool of inocula

To generate SICs in a straightforward, scalable, and reproducible manner, we focused on ex-germ-free mice colonized with human feces. These "humanized" mice facilitate controlled experimental manipulation within a mammalian host, enabling comparisons between *in vitro* and *in vivo* behaviors of communities of human commensals. We inoculated humanized mouse fecal samples into various media and repeatedly passaged in anaerobic batch cultures (Methods). We sought to inoculate with a set of fecal samples that varied widely in composition, yet were composed of the same set of members so that they could be readily compared.

We took advantage of our previous findings that diet and antibiotics have large, distinct, interacting effects on the composition of the microbiota (Ng et al., 2013; Sonnenburg et al., 2016). We inoculated 20 germ-free mice (5 per cage) with feces from a single human donor and allowed the microbiota to equilibrate for 6 weeks to allow for mucus normalization (Johansson et al., 2015). We shifted half of the mice (2 cages) from a standard diet (SD) to one deficient in microbiota-accessible carbohydrates (MD) and allowed the microbiota to re-equilibrate for two weeks. We then gavaged all mice (2 cages SD, 2 cages MD; n=20 total) for 5 days twice daily with 3 mg ciprofloxacin, which

bioRxiv preprint doi: https://doi.org/10.1101/2020.07.06.190181; this version posted July 6, 2020. The copyright holder for this preprint (which was not certified by peer review) is the author/funder. All rights reserved. No reuse allowed without permission.

inhibits bacterial type II topoisomerases such as *Escherichia coli* DNA gyrase. Since we previously showed that the responses of cage-mates to antibiotics are highly reproducible and stereotypical (Ng et al., 2019), we collected fecal samples from two randomly selected mice in different cages from each dietary condition on day 0 (pre-treatment) and on day 1 (peak of treatment, when the culturable load reached a maximum decrease of 10- to 100-fold (Ng et al., 2019)), day 5 (residual treatment, when ciprofloxacin was not being administered but was still detected in feces (Ng et al., 2019)), and day 14 (post-treatment) (Fig. 1A).

Using 16S sequencing and analysis (Methods), we quantified the relative abundances of amplicon sequence variants (ASVs, or unique sequences) and mapped them to taxa. SD mice underwent a substantial change in fecal-sample composition due to ciprofloxacin treatment, with consistent reductions in Bacteroidetes and Proteobacteria and expansions in Firmicutes and Verrucomicrobia at the peak of treatment (Fig. 1B, S1A). The relative abundance of the Bacteroidetes mostly returned to pre-treatment levels by day 5, while the Proteobacteria and Verrucomicrobia did not fully recover until day 14 (Fig. 1B, S1A). Fecal samples from MD mice showed similar trends but had lower levels of Bacteroidetes throughout the experiment (Fig. 1B, S1A).

For SD mice, the number of uniquely detected ASVs (richness) dropped from 91 to 68

bioRxiv preprint doi: https://doi.org/10.1101/2020.07.06.190181; this version posted July 6, 2020. The copyright holder for this preprint (which was not certified by peer review) is the author/funder. All rights reserved. No reuse allowed without permission.

on day 1 of treatment and to 19 by day 5 (Fig. S1B). Post-treatment diversity partially recovered to 56 ASVs (Fig. S1B). Richness dynamics were qualitatively similar for MD mice (Fig. S1B).

Principal coordinates analysis (PCoA, Methods) indicated that microbiota trajectories were distinct between dietary conditions (Fig. 1C). Thus, feces from humanized mice fed distinct diets and sampled at different timepoints during antibiotics treatment yielded an array of qualitatively different inocula. All these inocula were derived from the same human donor sample, enabling the generation of SICs with distinct starting compositions but with the potential for overlapping ASVs, facilitating the assessment of culturing conditions on a common pool of microbes.

In vitro *cultivation of stable SICs from fecal samples*

To generate SICs, we sampled mouse feces and quickly (<30 min after fecal pellet production) resuspended these 16 samples (2 diets, 4 treatment days, 2 mice per diet type) into media in anaerobic conditions and grew them in microplates in a plate reader at 37 ˚C (Methods, Fig. 1A). To explore multiple nutrient environments, we selected four common growth media: Brain Heart Infusion (BHI), Tryptone-Yeast extract-Glucose (TYG), Gifu Anaerobic Medium (GAM), and Yeast extract-Casitone-Fatty acids (YCFA). We inoculated three technical replicates of each resuspended fecal sample into

bioRxiv preprint doi: https://doi.org/10.1101/2020.07.06.190181; this version posted July 6, 2020. The copyright holder for this preprint (which was not certified by peer review) is the author/funder. All rights reserved. No reuse allowed without permission.

171 wells of each medium to test the replicability of the resulting SICs.

172

173 Nutrient supplies differ over time in the gut; hence, we grew SICs in anaerobic batch
174 culture rather than in a chemostat-like environment. Since some commensals require
175 >24 h to reach saturation (Tramontano et al., 2018), we allowed all cultures to grow for
176 48 h, before diluting them 200-fold into fresh medium. We repeated this cycle for 2-4
177 weeks (7-14 passages), and after each sub-culturing, we split the samples; half were
178 dedicated to glycerol frozen stocks and half to DNA extraction for 16S sequencing.
179 Passaged SICs were not frozen or exposed to oxygen at any point, and aside from the
180 brief period required for dilution, all samples were maintained at 37 ˚C throughout
181 passaging.

182

183 To determine whether SICs reached stable compositions, we first focused on 16S data
184 for the six SICs derived from pre-treatment samples from MD mice (Pre-MD) that were
185 grown in BHI. These samples underwent 16 passages rather than the typical 7, which
186 enabled us to identify whether changes in composition would occur over longer
187 timescales. At the family level, SICs stabilized by the second passage (Fig. 1D) and
188 retained most families from the original fecal sample (Fig. 1E). Of the families that were
189 present in the inoculum but not in the passaged SIC, most were at low abundance *in*
190 *vivo* (Fig. 1E); the lone exception was the Verrucomicrobiaceae, which were replaced by

bioRxiv preprint doi: https://doi.org/10.1101/2020.07.06.190181; this version posted July 6, 2020. The copyright holder for this preprint (which was not certified by peer review) is the author/funder. All rights reserved. No reuse allowed without permission.

Enterobacteriaceae in the SIC (Fig. 1D,E).

To quantify the relevance of SICs as a model for the gut microbiota, we introduced an SIC into germ-free mice. Families that were overrepresented *in vitro* receded *in vivo*, with family-level abundances similar to those of the humanized mice from which the SIC was derived (Fig. 1F, Fig. S1C). To evaluate effects on host physiology we quantified host and microbial proteins in the feces of three groups of mice: humanized mice, germ-free mice, and SIC-colonized mice. The host proteomes of SIC-colonized mice were more similar to those of humanized mice than to those of germ-free mice, and immunoglobulins were upregulated after colonization in SIC-colonized mice (Fig. S1D). In the SIC metaproteome, proteins from two of the most abundant bacterial species (determined via 16S sequencing) were present at levels similar to those in SIC-colonized and humanized mice (Fig. S1E). These findings demonstrate that top-down *in vitro* cultivation from fecal samples can deterministically select complex SICs that are stable under passaging for several weeks; re-introduction of SICs into a host re-establishes gut microbiota composition and promotes host homeostasis.

A previous soil and plant microbiota passaging study reported that despite convergence at the family level, genus-level composition was highly divergent across technical replicates (Goldford et al., 2018). In our experiments, family-level dynamics

bioRxiv preprint doi: https://doi.org/10.1101/2020.07.06.190181; this version posted July 6, 2020. The copyright holder for this preprint (which was not certified by peer review) is the author/funder. All rights reserved. No reuse allowed without permission.

were similar across all three replicate SICs from each of the two mice (Fig. S1F), as confirmed via PCoA (Fig. S1G). To test whether family-level replicability extended to the ASV level, we calculated the pairwise correlation coefficients of $\log_{10}$(relative abundance) between 7th passages of the 3 technical replicates of the SIC in Fig. 1D. Correlation coefficients and the percentage of ASVs shared (above 0.1% in both replicates) were uniformly high (Fig. 1G,H), and all ASVs that were present in only one replicate had relative abundance <1%. The three replicates contained 50 ASVs in total at >0.1%, which we define as a conservative measure of detectability, of which 14% were shared by exactly two replicates and 70% were shared by all three replicates. The 35 shared ASVs belonged to 9 families, 6 classes, and 3 phyla, and accounted for 97.5±1.1% (mean±standard deviation) of SIC total abundance. Hence, SIC replicability extends even to individual ASVs.

SICs were also reproducible across media and inocula (Fig. S1H, Supplementary Text). The lowest reproducibility was within SICs cultured in GAM and YCFA (Fig. S1I), where the dominance or absence of the Enterococcaceae explained most of the variation (Fig. S1J, Supplementary Text). Complex synthetic media mainly composed of amino acids and simple carbohydrates also drove the composition of SICs to be dominated by Enterococcaceae or Enterobacteriaceae (Fig. S1K). These findings indicate that *in vitro* culturing can lead to the selection of a few species in some media, and that SICs are

bioRxiv preprint doi: https://doi.org/10.1101/2020.07.06.190181; this version posted July 6, 2020. The copyright holder for this preprint (which was not certified by peer review) is the author/funder. All rights reserved. No reuse allowed without permission.

231 sometimes stochastic, even in media such as YCFA that promote the growth of many
232 commensals in isolation. These data also show that the SICs are generally diverse and
233 reproducible in BHI and TYG.
234
235 For steady-state SICs derived from feces to be useful for further experimentation, they
236 would ideally maintain their composition after freezing, and during growth in larger
237 volumes and without shaking. We inoculated the frozen stock from the 7th-passage SIC
238 in Fig. 1D (the last passage for which all other SICs in this work had frozen stocks, and a
239 passage in which all BHI communities had achieved stability, Fig. S1L) and grew it in a
240 15-fold larger volume (3 mL) of BHI in glass test tubes without shaking. The tube-
241 grown SIC had similar composition as the shaken SIC grown in a 96-well plate (Fig. 1I).
242 Thus, shaking is not required, allowing a large number of plates to be grown in an
243 incubator simultaneously, and large cultures can be readily produced.
244
245 To test SIC robustness to freezing, we inoculated -80 °C frozen stocks of the 3 mL test-
246 tube cultures directly into fresh BHI and passaged them for three additional 48-h cycles.
247 A single passage was sufficient to re-establish a composition closely matching that of
248 the 7th passage pre-freezing (Fig. 1J); 37 of 50 ASVs at >0.1% were retained and
249 accounted for 94.6% of the relative abundance pre-freezing. The composition was
250 unchanged after two additional passages (Fig. S2). All other tested communities grown

bioRxiv preprint doi: https://doi.org/10.1101/2020.07.06.190181; this version posted July 6, 2020. The copyright holder for this preprint (which was not certified by peer review) is the author/funder. All rights reserved. No reuse allowed without permission.

in BHI from other fecal inocula behaved similarly (Fig. S2), indicating that most taxa are preserved during freezing and thawing and that there were no substantive differential effects of freezing across taxa. Hence, SICs can be grown across a range of volumes, frozen, and revived without impact to the composition.

Initial inoculum composition and nutrient conditions affect SIC composition

To determine how quickly SICs converge, we computed the weighted Unifrac distance in ASV abundances (Methods) and determined when the distance decreased below 0.15 (the mean weighted Unifrac distance between technical replicates at the third passage). While a few SICs with low replicability also exhibited longer convergence timescales, the vast majority converged to a steady state within 4 passages (Fig. S1L).

To determine the extent to which the abiotic environment and inoculum dictated steady-state SIC compositions after 7 passages, we performed PCoA of our 16S data for all passages of all SICs in all media. The first coordinate was largely determined by the presence or absence of several co-occurring families, including Enterobacteriaceae (Fig. S3A). Most of these families were present in the pre-treatment inocula and were undetectable in residual treatment (day 5) inocula (Fig. S3B), suggesting that most of the variation is explained by the fecal inocula, not the culture media. Similar to previous studies of communities inoculated from soil and leaf samples (Goldford et al., 2018), our

bioRxiv preprint doi: https://doi.org/10.1101/2020.07.06.190181; this version posted July 6, 2020. The copyright holder for this preprint (which was not certified by peer review) is the author/funder. All rights reserved. No reuse allowed without permission.

data approximately clustered in the space of the first two principal coordinates according to culture media; BHI and TYG SICs overlapped but were well separated from GAM and even more so from YCFA (Fig. 2A). BHI, TYG, and GAM SICs were more similar to their inocula than YCFA SICs when using a weighted approach that accounts for taxonomical relative abundances (Fig. 2B). Using presence and absence of taxa as a measure of similarity (thus giving more weight to low-abundance taxa), BHI and TYG are better mimics of the conditions that produced the fecal pellet (Fig. 2A), regardless of the inoculating composition. The data also clearly clustered according to the time during antibiotic treatment when the inocula were sampled (Fig. 2A). Some SICs derived from the peak of antibiotic disturbance exhibited the largest differences from starting inoculum (Fig. 2A,C); instead, they more closely resembled SICs derived from residual treatment samples (Fig. 2A), likely due to low viable counts from samples at the peak of ciprofloxacin disturbance (Ng et al., 2019), implying that after antibiotic treatment, a fecal sample contains many non-viable cells. The direction separating clusters of sampling time was approximately orthogonal to the direction separating SICs by medium (Fig. 2A), indicating that both the availability of taxa in the inoculum and the ability of those taxa to grow as communities in a given medium dictate the composition of SICs.

SIC and fecal-sample richness are highly correlated due to maintenance of abundant

bioRxiv preprint doi: https://doi.org/10.1101/2020.07.06.190181; this version posted July 6, 2020. The copyright holder for this preprint (which was not certified by peer review) is the author/funder. All rights reserved. No reuse allowed without permission.

291 ***species and within-family replacement***

292 The presence or absence of multiple families in the first principal coordinate, and the
293 observation that this coordinate mainly separated SICs by their inocula (Fig. 2A),
294 suggested that SIC richness depends on the richness of the inoculum. Indeed, the first
295 principal coordinate was correlated with inoculum richness (Fig. S3C), and the richness
296 of SICs grown in BHI, TYG, and GAM was highly correlated with that of the inoculum,
297 with some SICs having >50 detectable ASVs (Fig. 2D). These SICs showed similar
298 evenness (relative abundance homogeneity) as their inocula (Fig. S4A). SICs grown in
299 YCFA exhibited very low diversity and extreme evenness (Fig. 2D, S4A).

300

301 The total number of ASVs present in at least one inoculum was 158, and the total
302 number of ASVs present in at least one SIC was 117. Nevertheless, only 79 of the 158
303 ASVs (50%) present in the inocula were present in at least one SIC, indicating
304 emergence of some ASVs from below the limit of detection (Supplementary text). Most
305 of the retained ASVs (68 of 79) were present in at least one BHI SIC. While fecal
306 diversity was approximately maintained in SICs (Fig. 2D) and family-level composition
307 was preserved for families conducive to culturing (Fig. 1D, 2A), passaging led to a
308 reproducible decrease of some ASVs to below the limit of detection; this decrease was
309 biased toward ASVs that started at lower abundance and was mostly balanced by
310 emergent ASVs from the same family (Supplementary text). The only family to emerge

bioRxiv preprint doi: https://doi.org/10.1101/2020.07.06.190181; this version posted July 6, 2020. The copyright holder for this preprint (which was not certified by peer review) is the author/funder. All rights reserved. No reuse allowed without permission.

311 above the limit of detection during passaging was the sole Gammaproteobacterial
312 family (an Enterobacteriaceae). Nonetheless, the Enterobacteriaceae emerged almost
313 exclusively in SICs derived from pre- and post-treatment inocula (Fig. S1M), indicating
314 that this emergence was not due to contamination. Thus, both maintenance and within-
315 family replacement contribute to SIC richness at steady state.
316
317 ***SIC growth dynamics reflect compositional characteristics***
318 We speculated that SIC characteristics such as richness and the presence or absence of
319 key species may be reflected in the features of continuous growth curves. We first
320 focused on BHI SICs since they harbored the highest diversity (Fig. 2D). We measured
321 SIC optical densities (ODs) at 20 h ("yield") because by that time all growth rates had
322 become virtually zero. We averaged the last 4 passages for each condition and sample
323 and found a range of mean final ODs that were highly correlated with SIC richness
324 (R=0.92, p=6×10^{-30}; Fig. 2E). Similar relationships held for TYG and GAM (Fig. S5A).
325 Thus, the yield of these SICs was greater when more taxa are present, suggesting that in
326 the appropriate medium, SICs with low diversity could support the growth of more
327 taxa if they were present in the inoculum.
328
329 We next calculated the maximum growth rate (Methods) for each SIC and again
330 observed that richness correlated with maximum growth rate (R=0.50, p=2.7×10^{-4}, Fig.

bioRxiv preprint doi: https://doi.org/10.1101/2020.07.06.190181; this version posted July 6, 2020. The copyright holder for this preprint (which was not certified by peer review) is the author/funder. All rights reserved. No reuse allowed without permission.

S5B). The distribution of maximum growth rates was bimodal, reaching as high as 1.7 h^{-1} (doubling time ~25 min) (Fig. S5B), similar to the growth rates of fast-growing species such as *E. coli* in rich media (Baev et al., 2006). We hypothesized that the presence of those families would correlate with SIC maximum growth rate. The summed relative abundance of the two families (f_{Entero}) was also bimodal and correlated with maximum growth rate (Fig. S5C). SICs with $f_{Entero} > 20\%$ had a significantly higher maximum growth rate (Fig. 2F). Yield (Methods) was also linked to the presence of Enterobacteriaceae and Enterococcaceae after 48 h of growth (Fig. 2G). These correlations were similar in TYG and GAM (Fig. S5D), indicating that the relationship between these families and growth rate is likely medium-independent.

In YCFA, there was no correlation between richness and final OD (Fig. S5A), probably due to the overall low diversity of these SICs. Nonetheless, the relative abundance of fast growers was still linked to maximum growth rate (Fig. S5D). Some YCFA technical replicates that diverged in composition during passaging exhibited blooming of an *Enterococcus* species in the sixth passage in two of three replicates (Fig. S1Jiii). This bloom coincided with a change in maximum growth rate (Fig. 2H,I), suggesting that growth features can also be used to dynamically detect major changes in composition *in vitro*.

bioRxiv preprint doi: https://doi.org/10.1101/2020.07.06.190181; this version posted July 6, 2020. The copyright holder for this preprint (which was not certified by peer review) is the author/funder. All rights reserved. No reuse allowed without permission.

351 ***The population growth behavior of SICs can be partially reconstituted using isolates***

352 Ideally, our top-down approach to SIC cultivation could be complemented with
353 bottom-up reconstitution using isolates. We focused on an SIC cultured in BHI from a
354 MD mouse pre-treatment (Pre-MD) inoculum (parent SIC, Fig. 1D,3A) based on its high
355 diversity (>50 ASVs, Fig. 2D). We obtained 15 distinct isolates by plating and analyzing
356 192 colonies (Fig. 3A, Methods). While these isolates represented <30% of the total
357 number of ASVs in the parent SIC, they accounted for 69% of its total abundance (Fig.
358 3B). Our isolates included the sole Enterococcaceae, Porphyromonadaceae, and
359 Enterobacteriaceae ASVs present at >0.1% in the parent SIC (Fig. 3B).

360

361 To test whether these 15 isolates were sufficient to recapitulate the growth and
362 composition of the parent SIC, we examined the growth behaviors of our parent SIC, as
363 well as the isolates alone and in a reconstituted SIC (Fig. 3A). We grew each isolate from
364 frozen stock in the medium from which it was isolated at 37 °C for 48 h. We then
365 passaged the isolates individually in BHI and measured OD over time to quantify lag
366 time, maximum growth rate, and yield. *Enterococcus* and *Escherichia* strains had higher
367 maximum growth rates and shorter lag times than the other isolates (Fig. 3C,D), and
368 were relatively abundant in the parent SIC (7.6±0.8% and 15.1±0.1%, respectively; n=3,
369 Fig. 3B). While the initial phase of growth after subculturing is likely dominated by
370 these fast-growing species, the parent SIC grew significantly slower than the three

bioRxiv preprint doi: https://doi.org/10.1101/2020.07.06.190181; this version posted July 6, 2020. The copyright holder for this preprint (which was not certified by peer review) is the author/funder. All rights reserved. No reuse allowed without permission.

371 *Enterococcus* isolates (all of which were represented by the same ASV) and *Escherichia*
372 *fergusonii* (Fig. S6A); the lag time of the parent SIC was higher than the shortest isolate
373 lag time (*E. fergusonii*) (Fig. S6B). Isolate yield was more homogeneous (Fig. 3E).
374 Although some of the poorest growers were *Bacteroides thetaiotaomicron* and
375 *Parabacteroides distasonis* (final ODs 0.032±0.004 and 0.010±0.006, respectively, Fig. 3C),
376 the corresponding ASVs ended up as 13.23±0.6% and 1.7±0.1% of the parent SIC,
377 respectively, suggesting that their growth is not greatly hampered by the initial
378 expansion of other species.
379
380 We built a reconstituted SIC (Fig. 3A) by growing the 15 isolates independently to
381 saturation, diluting them to OD=0.001 in BHI, and mixing them in equal volumes. To
382 test whether other strains slowed the growth of *Enterococcus* spp. and *E. fergusonii* in the
383 parent SIC, we monitored growth at 37 °C for 48 h and then passaged this reconstituted
384 SIC twice more. The reconstituted SIC had a higher maximum growth rate but the same
385 lag time as its parent SIC in the third passage (Fig. 3F, S6C). Thus, fast-growing species
386 likely expand initially in the absence of competition for nutrients, reshaping the niche
387 landscape, after which slower-growing species fill unoccupied or new niches and
388 enforce physiological states on the fast-growing species that make them unable to grow
389 as quickly in subsequent passages despite their higher relative abundance. Supporting
390 this notion, the yield of the parent SIC was higher than that of the reconstituted SIC in

bioRxiv preprint doi: https://doi.org/10.1101/2020.07.06.190181; this version posted July 6, 2020. The copyright holder for this preprint (which was not certified by peer review) is the author/funder. All rights reserved. No reuse allowed without permission.

391 the third passage (Fig. 3G); this increase was realized during entry to stationary phase
392 (Fig. S6D), indicating that the other, unisolated species were slow growers that occupy
393 niches not filled by the isolates. Both sets of species contribute to yield and further
394 depress maximum growth rate.
395
396 Are the growth properties of reconstituted SICs general to the component species or
397 specific to isolated strains? We built an SIC with the closest relatives of each of the 15
398 isolates that were available in reference strain collections (reference SIC, Fig. 3A) and
399 monitored growth of the reference strains for one passage and of the reference SIC for
400 three passages. The maximum growth rate of the isolates and their closest relative
401 reference strains grown alone were highly correlated (Fig. S6E); the reference SIC had
402 the same maximum growth rate (Fig. 3E) and a longer lag phase (Fig. S6C) than the
403 reconstituted SIC. However, the reference SIC yield was substantially lower than that of
404 the reconstituted SIC and the parent SIC (Fig. 3G), likely because *E. fergusonii* had the
405 highest yield of all isolates but the corresponding reference strain exhibited a much
406 lower yield in BHI (Fig. 3H). Hence, the ability of co-cultures to recapitulate a complex
407 SIC can depend on community effects (growth rate) and metabolic properties of
408 individual strains (yield).
409
410 To test how much the composition of reconstituted and reference SICs resembled that of

bioRxiv preprint doi: https://doi.org/10.1101/2020.07.06.190181; this version posted July 6, 2020. The copyright holder for this preprint (which was not certified by peer review) is the author/funder. All rights reserved. No reuse allowed without permission.

411 the parent SIC, we performed 16S amplicon sequencing (Methods). The reconstituted
412 and reference SICs mostly stabilized within one passage (Fig. 3I). In general, the relative
413 abundances of the ASVs in the reconstituted and reference SICs were highly correlated
414 with those in the parent SIC (Fig. 3J,K), but not with isolate yields or maximum growth
415 rates (Fig. 3L,M). The family-level relative abundances in reconstituted and reference
416 SICs were correlated (Fig. S6F). Notably, even though *E. fergusonii* and *Enterococcus* spp.
417 can grow more quickly and more than most other isolates (Fig. S6E), their overall
418 contributions to co-culture yield were limited by the other species. Moreover, the
419 similarly high abundances of the 3 *Bacteroides* species (despite all but *B. fragilis* being
420 poor growers in isolation in unsupplemented BHI, Fig. S6E) suggests that some
421 *Bacteroides* rely on other organisms for optimal growth. Overall, co-culturing these 15
422 species seems to reproduce much of the metabolic web responsible for establishing their
423 abundances in the parent SIC.
424
425 ***Ciprofloxacin alters SICs in a manner generally consistent with isolate sensitivities***
426 We queried the responses of our SICs to ciprofloxacin. We selected an SIC derived from
427 an inoculum that had not been exposed to the drug *in vivo* (pre-treatment from SD
428 mouse, Pre-SD, Fig. 4A). We grew a frozen stock in BHI for 48 h over two rounds of
429 passaging and then diluted 1:200 into a 96-well plate in duplicate with increasing
430 ciprofloxacin concentrations (Fig. 4Ai). The maximum growth rate of the SICs decreased

bioRxiv preprint doi: https://doi.org/10.1101/2020.07.06.190181; this version posted July 6, 2020. The copyright holder for this preprint (which was not certified by peer review) is the author/funder. All rights reserved. No reuse allowed without permission.

monotonically with drug concentration (Fig. 4B) and the collective minimum inhibitory concentration (MIC) for the SIC was >32 μg/mL (Fig. 4B). The final OD of the Pre-SD SIC exhibited at least two notable decreases, at the lowest and highest concentrations (Fig. 4B); our findings (Fig. 2A) suggest that these decreases are due to drops in diversity. To test the effects of long-term exposure to ciprofloxacin, we passaged the Pre-SD SICs in BHI with the ciprofloxacin concentrations to which they were exposed in the first passage for two more *in vitro* passages (Fig. 4Aii,iii). For the highest concentrations, the maximum growth rate increased moderately after the first passage (Fig. 4C). The increasing growth rate upon additional passages in antibiotic suggest that the structure of the SIC changes after *in vitro* treatment, potentially due to selection of resistant subpopulations.

To assess compositional changes in the Pre-SD SIC upon treatment, we performed 16S sequencing after 48 h of treatment with 2, 8, and 32 μg/mL ciprofloxacin in each of the three consecutive passages (Fig. 4Ai,ii,iii). At 2 μg/mL, diversity of the Pre-SD SIC decreased relative to the untreated SIC in the first passage (Fig. 4D). At 32 μg/mL, the diversity of the Pre-SD SIC declined to levels lower than those of SICs derived from residual-treatment inocula of the same SD mouse in the absence of ciprofloxacin (Fig. 2D, 4D), suggesting that the 2-32 μg/mL range encompasses those experienced by the microbiota *in vivo*. For all doses, many families in the Pre-SD SIC decreased to

bioRxiv preprint doi: https://doi.org/10.1101/2020.07.06.190181; this version posted July 6, 2020. The copyright holder for this preprint (which was not certified by peer review) is the author/funder. All rights reserved. No reuse allowed without permission.

451 undetectable levels, including the abundant Enterobacteriaceae and Enterococcaceae
452 (Fig. 4E), consistent with the drop in maximum OD relative to the untreated SIC (Fig.
453 2G, 4B). Members of the Lachnospiraceae, Ruminococcaceae, and Bacteroidaceae
454 persisted after three rounds in 2 and 8 μg/mL ciprofloxacin (Fig. 4E). At 32 μg/mL, the
455 Ruminococcaceae were undetectable by the second passage and the Bacteroidaceae
456 decreased to very low levels (Fig. 4E), likely explaining the large decrease in maximum
457 OD relative to 16 μg/mL (Fig. 4B).
458
459 Next, we examined changes at the ASV level to assess within-family dynamics. In the
460 Pre-SD SIC, antibiotic pressure can select for strains that emerge from below the
461 detection limit due to the decrease of other, more sensitive species: at 2 μg/mL the
462 Lachnospiraceae increased from 12 to 16 detectable ASVs while the Bacteroidaceae
463 decreased from 12 to 4 detectable ASVs. At every concentration, the changes were
464 highly reproducible between replicates (more than 89% and 69% of ASVs that became
465 undetectable or detectable, respectively, did so in both replicates). To test whether the
466 observed changes were explained by the sensitivities of each family to ciprofloxacin, we
467 measured the MIC of the 15 strains isolated from a Pre-MD SIC (Fig. 3A, Table S1). The
468 isolate MICs were highly correlated with the fractional change in abundance upon 2
469 μg/mL ciprofloxacin treatment of the Pre-SD SIC (Fig. 4F). These data show that the
470 compositional changes observed in SICs can largely be predicted by individual

bioRxiv preprint doi: https://doi.org/10.1101/2020.07.06.190181; this version posted July 6, 2020. The copyright holder for this preprint (which was not certified by peer review) is the author/funder. All rights reserved. No reuse allowed without permission.

sensitivities in isolation.

SICs can predict in vivo *compositional changes due to ciprofloxacin*

While a drug concentration can be measured in fecal samples, it is usually undetermined along the gastrointestinal tract and potentially heterogeneous in space and time. Other variables are currently impossible to measure and control, such as environmental reservoirs that could play a role in bacterial migration and repopulation. Our SICs provide the opportunity to study antibiotic perturbations in a precisely controlled and high-throughput manner, to assess similarity to *in vivo* behavior, and to interpret changes *in vivo* mechanistically.

Humanized mice treated with ciprofloxacin harbored high levels of Lachnospiraceae and Ruminococcaceae at the peak of treatment (Fig. S1A), in agreement with the selection of these families in SICs (Fig. 4E). Of the families for which we obtained MICs (Table S1), the highest MIC was observed in the Lachnospiraceae, and this family remained high or increased in relative abundance upon residual treatment *in vivo* (Fig. 5A). Most sensitive families (MIC <32 μg/mL) decreased in abundance (Fig. 5A, Fig. S1M); the lone exception was the Bacteroidaceae, which increased in three of four mice (Fig. 5A), consistent with our previous observation that a highly resistant *Bacteroides vulgatus* strain (MIC >512 μg/mL) can be selected *in vivo* (Ng et al., 2019). Again, these

bioRxiv preprint doi: https://doi.org/10.1101/2020.07.06.190181; this version posted July 6, 2020. The copyright holder for this preprint (which was not certified by peer review) is the author/funder. All rights reserved. No reuse allowed without permission.

491 results suggest that the effective concentration *in vivo* is between 2 and 32 μg/mL. These
492 similarities suggest that ciprofloxacin sensitivities are generally similar *in vitro* and *in*
493 *vivo*, and that individual sensitivities largely dictate the initial dynamics of SIC
494 composition *in vivo*.
495
496 *In vivo*, the microbiota undergoes a complex recovery that likely involves differential
497 susceptibilities, intrinsic recovery capacities, the emergence of resistant mutants, and
498 metabolic interactions (Ng et al., 2019). To investigate the response of SICs in conditions
499 resembling recovery from treatment *in vivo*, we diluted the Pre-SD SIC into plates
500 without ciprofloxacin after one round in ciprofloxacin (Fig. 5Bi,iv,v). The Pre-SD SIC
501 exhibited increases in maximum growth rate after one round of treatment at all doses
502 (Fig. 5C); at low doses, growth rate rebounded to values similar to those before
503 treatment, while at >8 μg/mL it only partially recovered (Fig. 5C). All the doses at which
504 maximum growth rate increased back to similar levels to those before treatment
505 showed recovery of the Enterococcaceae (Fig. S7A), in line with the correlation of the
506 presence of this family and maximum growth rate (Fig. 2B) and the MIC of *Enterococcus*
507 isolates (2-4 μg/mL, Table S1). Removal of the drug slightly increased diversity in Pre-
508 SD SICs (Fig. 5D), indicating that the recovery of certain species drives the partial
509 recovery of growth rate. Thus, diversity recovery *in vitro* and *in vivo* (Fig. S1B) can be
510 partially explained by re-emergence of ASVs that became undetectable during

bioRxiv preprint doi: https://doi.org/10.1101/2020.07.06.190181; this version posted July 6, 2020. The copyright holder for this preprint (which was not certified by peer review) is the author/funder. All rights reserved. No reuse allowed without permission.

511 treatment.

512

513 We next computed the extent of compositional disruption during treatment and the
514 degree of recovery after treatment based on the Bray-Curtis dissimilarity index.
515 Ciprofloxacin dose determined the dissimilarity between the Pre-SD SIC before
516 treatment and after three passages in ciprofloxacin (Fig. 5E). The compositions of the
517 treated SICs were highly reproducible at the ASV level, especially at low concentrations
518 (Fig. S7B). After removing the drug from the highest-concentration conditions, the SICs
519 became more similar to, although still differed substantially from, the untreated state
520 (Fig. 5E). Interestingly, at lower concentrations the dissimilarity increased after removal
521 of the drug (Fig. 5E) due to the survival and expansion of taxa that were present at very
522 low abundance before ciprofloxacin treatment. This non-monotonic dose-response is
523 reminiscent of the better recovery of the microbiota in mice during high-dose compared
524 with low-dose osmotic diarrhea (Tropini et al., 2018). SICs hence adopt a new steady
525 state after ciprofloxacin exposure and recovery, as we previously observed *in vivo* (Ng
526 et al., 2019).

527

528 The small increase in SIC diversity after ciprofloxacin removal (Fig. 5D) was associated
529 with the recovery of Erysipelotrichaceae, Ruminococcaceae, and Enterococcaceae
530 members from below the limit of detection (Fig. 5F). The Erysipelotrichaceae family

bioRxiv preprint doi: https://doi.org/10.1101/2020.07.06.190181; this version posted July 6, 2020. The copyright holder for this preprint (which was not certified by peer review) is the author/funder. All rights reserved. No reuse allowed without permission.

recovered from one treatment at all concentrations (Fig. 5F), consistent with its recovery *in vivo* post-treatment (Fig. S1A). A second treatment after one passage without the drug (Fig. 5Bvi) again made the Erysipelotrichaceae undetectable (Fig. S7C), indicating that sensitivity to ciprofloxacin was the same before and after one treatment-recovery cycle. The other families did not recover from undetectable levels after removing the drug (Fig. 5F). Of the families that became undetectable, the only one to exhibit different recovery characteristics *in vitro* and *in vivo* (Fig. 5F,G,H, S7D) was the Bacteroidaceae, which were undetectable at 32 μg/mL ciprofloxacin *in vitro* but persisted *in vivo*. Taken together, these results show that *in vitro* perturbations can be used as a proxy for many aspects of *in vivo* dynamics.

Bacteroides *recovery* in vitro *is due to a combination of resistance and resilience*

The unexpected recovery of the Bacteroidaceae *in vivo* motivated us to probe the dynamics of these ASVs. *In vivo*, although most *Bacteroides* ASVs were undetectable at the peak and residual time points, most reappeared post-treatment (Fig. 5I, S7E). Only *B. vulgatus* in relative abundance to become dominant during residual treatment (Fig. 5I, S7E); this strain was likely highly resistant to ciprofloxacin based on our assessment of *Bacteroides* isolates from the residual fecal sample (Ng et al., 2019). Consistent with this observation, *B. vulgatus* was the only Bacteroidaceae ASV that was present *in vitro* after 3 passages with 32 μg/mL ciprofloxacin, reaching a stable abundance (Fig. 5J). *B.*

bioRxiv preprint doi: https://doi.org/10.1101/2020.07.06.190181; this version posted July 6, 2020. The copyright holder for this preprint (which was not certified by peer review) is the author/funder. All rights reserved. No reuse allowed without permission.

551 *caccae* and *B. uniformis* were present after 3 passages at 8 μg/mL, and *B. thetaiotaomicron*
552 was present after 3 passages at 2 μg/mL (Fig. 5J); all three species recovered *in vivo* post-
553 treatment (Fig. 5I). Other *Bacteroides* spp., such as *B. fragilis*, became undetectable after
554 one passage at 2 μg/mL (Fig. 5J). These trends are consistent with the higher MICs of *B.*
555 *uniformis* and *B. thetaiotaomicron* compared to *B. fragilis* (Table S1). Thus, sensitivities of
556 isolates are predictive of *Bacteroides* resistance during continuous ciprofloxacin
557 treatment in SICs.
558
559 Like *B. fragilis*, *B. intestinalis* was undetectable by the second passage even at the lowest
560 ciprofloxacin concentration tested *in vitro* (Fig. 5J). Nonetheless, both species recovered
561 *in vivo* in SD mice (Fig. 5I). Remarkably, these species also re-emerged *in vitro* when
562 ciprofloxacin-treated SICs were diluted into medium without the drug (Fig. 5K). *B.*
563 *fragilis* increased in relative abundance and became dominant after treatment with 2
564 μg/mL (Fig. 5K), while *B. intestinalis* was detected only after 8 μg/mL (Fig. 5K),
565 suggesting that competition with other species or taxa at the lower concentration drove
566 *B. intestinalis* to undetectable levels. After treatment with 32 μg/mL, no *Bacteroides*
567 species recovered (Fig. 5K). We refer to the ability of these strains to recover from
568 undetectable levels during treatment as "resilience". Interestingly, *B. vulgatus* was only
569 detected when the SIC was continuously exposed (Fig. 5J) and not after ciprofloxacin
570 was removed (Fig. 5K), suggesting that the recovery of other taxa can drive resistant

bioRxiv preprint doi: https://doi.org/10.1101/2020.07.06.190181; this version posted July 6, 2020. The copyright holder for this preprint (which was not certified by peer review) is the author/funder. All rights reserved. No reuse allowed without permission.

571 members to undetectable levels. Species that did not recover *in vivo*, such as *B. ovatus*,
572 did not recover *in vitro* (Fig. 5I,K). These data demonstrate that fecal-derived SICs can
573 recapitulate species-level dynamics observed *in vivo* and can distinguish between
574 resistance and resilience. Our observations of species resilience within complex SICs
575 also show that re-seeding from environmental reservoirs is not necessary for species to
576 recover after antibiotic treatment.
577
578 ***Exposure to ciprofloxacin* in vivo *leads to functional differences* in vitro**
579 The compositions of SICs derived during and after antibiotic treatment resembled the
580 compositions of the inocula (Fig. 2A,C). Thus, we next asked whether the SICs retained
581 functions observed *in vivo*: decreased resistance to colonization by the pathogen
582 *Salmonella enterica* serovar Typhimurium (Barthel et al., 2003; Lawley et al., 2008) and
583 increased resilience to a second round of treatment (Ng et al., 2019).
584
585 First, we asked whether exposure to ciprofloxacin led to compositional changes that
586 reduce colonization resistance in the absence of the drug *in vitro*. We grew SICs derived
587 from SD mice inocula gathered before, during the peak of, during residual, and after
588 treatment *in vivo* (Pre-SD, Peak-SD, Res-SD, and Post-SD, respectively, Fig. 6A) in BHI.
589 We challenged these SICs with *S.* Typhimurium for 48 h in BHI, diluted them, spotted
590 them onto LB-streptomycin agar plates, and incubated them in aerobic conditions to

bioRxiv preprint doi: https://doi.org/10.1101/2020.07.06.190181; this version posted July 6, 2020. The copyright holder for this preprint (which was not certified by peer review) is the author/funder. All rights reserved. No reuse allowed without permission.

591 select for *S.* Typhimurium. Pre-SD SICs had >10-fold less *S.* Typhimurium than
592 communities derived from feces of ciprofloxacin-treated mice (Fig. 6B, S8A). Single-cell
593 quantification of fluorescently tagged *S.* Typhimurium revealed an even larger
594 difference in colonization efficiency between the Pre-SD and Res-SD SICs (Fig. 6C, S8B).
595 Thus, changes in composition driven by antibiotic treatment *in vivo* lead to differences
596 in SICs that mimic the resilience of the microbiota to pathogen invasion *in vivo*.
597
598 Second, we asked whether the pre-exposed, low-diversity Res-SD SIC showed higher
599 resilience to ciprofloxacin *in vitro* than the Pre-SD SIC (Fig. 6D). We grew the SICs in
600 BHI with ciprofloxacin continuously (Fig. 6Di,ii,ii) or transiently (Fig. 6Di,iv,v) as
601 above. The Res-SD SIC was less sensitive than the Pre-SD SIC in terms of growth rate
602 (Fig. 4B, 6E), and the final OD was largely unaffected (Fig. 6E).
603
604 We next asked whether the robustness of Res-SD SIC growth behaviors (Fig. 6E) during
605 ciprofloxacin treatment could be explained by particular compositional differences from
606 the Pre-SD SIC. The Res-SD SIC displayed responses distinct from those of the Pre-SD
607 SIC, maintaining diversity even at the highest ciprofloxacin concentrations (Fig. 4C, 6F).
608 At all concentrations, Bacteroidaceae and Lachnospiraceae dominated even after three
609 passages (Fig. 6G), in contrast to the elimination of most Bacteroidaceae in the Pre-SD
610 SIC (Fig. 4E). The most abundant family that was subsequently lost from Res-SD SIC

bioRxiv preprint doi: https://doi.org/10.1101/2020.07.06.190181; this version posted July 6, 2020. The copyright holder for this preprint (which was not certified by peer review) is the author/funder. All rights reserved. No reuse allowed without permission.

611 was the Enterococcaceae (Fig. 6G); the Ruminococcaceae and Verrucomicrobiaceae were
612 lost at 32 and 2 μg/mL ciprofloxacin, respectively (Fig. 6G). These losses were
613 counterbalanced by emergent ASVs within the resistant families. As with the Pre-SD
614 inocula, composition was quantitatively similar at the ASV level between the two
615 replicates at low ciprofloxacin concentrations (Fig. S7G). At 32 μg/mL, the two
616 replicates were more similar to each other than to the Pre-SD SIC after treatment (Fig.
617 S7D), suggesting that pre-exposure to the drug in mice decreases the stochastic nature
618 of species elimination upon subsequent exposure *in vitro*.
619
620 The compositions of the Res-SD SIC before treatment and after two recovery passages
621 were highly similar at low doses (Fig. 6H). For all doses, the dissimilarity index of the
622 post-recovery Res-SD SIC reverted toward its original state (Fig. 6I); by contrast, at 2
623 μg/mL ciprofloxacin, the Pre-SD SIC was further remodeled during recovery (Fig. 5E).
624 These data imply that the members of the Res-SD SIC are more resistant to the drug
625 than members of the Pre-SD SIC, in line with their pre-selection *in vivo*.
626
627 Both *in vitro* for the Pre-SD SIC and *in vivo*, we observed selection of *B. vulgatus* upon
628 treatment with ciprofloxacin (Fig. 5I,J). However, in the absence of ciprofloxacin, *B.*
629 *fragilis* dominated the Bacteroidaceae of the Res-SD SIC (Fig. 6J), consistent with this
630 species' ability to recover and dominate the Pre-SD SIC after ciprofloxacin removal (Fig.

bioRxiv preprint doi: https://doi.org/10.1101/2020.07.06.190181; this version posted July 6, 2020. The copyright holder for this preprint (which was not certified by peer review) is the author/funder. All rights reserved. No reuse allowed without permission.

5K), while *B. vulgatus* and *B. caccae* were at low relative abundances (Fig. 6J). *B. fragilis* became undetectable during Res-SD treatment regardless of concentration, as did *B. caccae* at 32 μg/mL (Fig. 6J). *B. vulgatus* accounted for the totality of the Bacteroidaceae at 32 μg/mL (~20% of the SIC; Fig. 6G,J). At 2 μg/mL, the *B. fragilis* ASV re-emerged after two recovery passages in one replicate at the expense of *B. vulgatus* (Fig. 6K), similar to the replacement of the resistant *B. vulgatus in vivo* by other *Bacteroides* (Fig. 5I). Thus, SICs derived from residual inocula are generally more resilient to ciprofloxacin and exhibited *Bacteroides* dynamics similar to *in vivo* treatment. These data suggest that the initial treatment culls the community down to a resistant core, leading to a community that is stable under further treatment.

Diverse, stable SICs can be generated directly from human fecal samples

Our experiments consistently showed that passaging of fecal samples from humanized mice can lead to stable SICs preserving many of the taxa from the original sample. What about feces sampled directly from humans? Three human stools from anonymous donors were more diverse than the humanized mice fecal samples (Fig. 2D,S1B), with 115-219 ASVs. We passaged the samples in BHI and observed trends of rapid convergence to a stable steady state and high family-level diversity similar to SICs derived from humanized mice (Fig. 7A); SIC composition stabilized in 3.1±0.3 passages, and the mean richness after the 8th passage was 46.4±2.4 ASVs (n=3).

bioRxiv preprint doi: https://doi.org/10.1101/2020.07.06.190181; this version posted July 6, 2020. The copyright holder for this preprint (which was not certified by peer review) is the author/funder. All rights reserved. No reuse allowed without permission.

651

652 Steady-state compositions of the passaged SICs were reproducible across technical
653 replicates (Fig. S9A), but across donors, the SICs differed at the family level, with >50%
654 of families being unique to one donor (Fig. 7A, S9B). Of the 103 unique ASVs across all
655 human stool-derived SICs, only 9 were shared among SICs derived from all three
656 donors (6 *Bacteroides* spp., 1 Lachnospiraceae, 1 Enterobacteriaceae, 1
657 Ruminococcaceae). Families that were shared among the three human stool-derived
658 SICs were highly overlapping with those of the core microbiota from our other
659 humanized mouse-derived passaged SICs (Fig. 7B, S9C). Moreover the relative
660 abundances of these ASVs were similar in all human stool-derived SICs (Fig. S9B).

661

662 To compare to humanized mouse SICs, we performed a PCoA on humanized mouse
663 and human stool SICs together, considering the presence or absence of ASVs
664 (unweighted Unifrac distances, Fig. 7C). SICs from two stool samples had phylogenetic
665 compositions (weighted Unifrac distances) similar to those of their inocula (the
666 corresponding human stool sample), while the third sample was more different from
667 the final SICs (Fig. 7D) due largely to the emergence of the Eubacteriaceae and
668 Enterococcaceae from undetectable to 0.29±0.13% and 4.9±1.1%, respectively.
669 Nonetheless, the final SICs derived from human stool after 7 passages were as (or more)
670 similar to their inocula than the humanized mouse-derived SICs were to their inocula

bioRxiv preprint doi: https://doi.org/10.1101/2020.07.06.190181; this version posted July 6, 2020. The copyright holder for this preprint (which was not certified by peer review) is the author/funder. All rights reserved. No reuse allowed without permission.

671 (the corresponding mouse fecal sample) using phylogenetic distance metrics (Fig.
672 7C,D). Taken together, these data demonstrate that *in vitro* batch culturing of human
673 stool samples is a generally applicable tool to build complex, stable, and reproducible
674 SICs.

bioRxiv preprint doi: https://doi.org/10.1101/2020.07.06.190181; this version posted July 6, 2020. The copyright holder for this preprint (which was not certified by peer review) is the author/funder. All rights reserved. No reuse allowed without permission.

675 **Discussion**

676 Here, we have shown that *in vitro* passaging of fecal samples is a powerful tool for
677 generating stable, host-relevant SICs in a deterministic and reproducible manner (Fig.
678 1G,H,S2A). Remarkably, this reproducibility even extends to a highly perturbative
679 antibiotic treatment that causes large-scale compositional changes (Fig. S7B,G). SICs
680 rapidly converge (Fig. 1D,S1L) and can be frozen (Fig. 1J) and cultured in larger
681 volumes (Fig. 1I) without disrupting steady-state composition, demonstrating their
682 utility for large-scale manufacturing and experimentation. Particular media may be
683 useful for enhancing the abundance of certain desired families, while antibiotics and
684 bacteriophages may be useful to remove undesirable taxa. Importantly, our observation
685 that different inocula yield different SICs (Fig. 2, 7) showcases the potential of SICs for
686 personalized therapeutics.

687

688 While our approach yields SICs that are more complex than ones typically studied with
689 bottom-up approaches, the scaling of richness with growth yield (Fig. 2E) suggests that
690 niche occupancy in BHI is saturated at ~50 species, leading to competitive exclusion
691 (Del Monte-Luna et al., 2004). It will be intriguing to investigate whether it is possible to
692 achieve higher richness in other media, or by supplementing BHI with vitamins,
693 cofactors, or specific nutrients such as mucin to promote the growth of fastidious
694 organisms (Tramontano et al., 2018), like the Verrucomicrobia. Cross-feeding may

bioRxiv preprint doi: https://doi.org/10.1101/2020.07.06.190181; this version posted July 6, 2020. The copyright holder for this preprint (which was not certified by peer review) is the author/funder. All rights reserved. No reuse allowed without permission.

increase richness and reshape community composition via niche generation (Goldford et al., 2018). Conversely, media composed of monomeric and dimeric carbon sources that are absorbed in the small intestine select for a few dominant species (Fig. S1K). A better understanding of the contributions of interspecies interactions and nutrient availability to community diversity and yield will be instrumental to engineering culturing systems to achieve the bacterial density and diversity observed in the gut. Our SICs represent a major step toward this goal.

Strikingly, while YCFA supports the growth of a wide range of gut commensals in pure cultures, in SICs the Enterococcaceae tend to take over (Fig. S1J, S3A), indicating that media that support the growth of many isolates do not necessarily support diverse SICs. Further, the ability of species to grow in isolation is generally not a good predictor of their relative abundance within an SIC (Fig. 3L). While the maximal growth rate of SICs scales with the fraction of fast growers (Fig. 2F), fast growers are quickly limited (Fig. 3M). Thus, fast growers probably dictate SIC growth rate, but final composition is determined by many other factors, which explains why BHI SICs are far more diverse than a scenario in which the rapid growers take over. Measurements beyond SIC composition—such as consumption and production of metabolites, growth and death rates of species, and global environmental properties such as pH and osmolarity—will enable a mechanistic understanding of community niche dynamics. Since SIC

bioRxiv preprint doi: https://doi.org/10.1101/2020.07.06.190181; this version posted July 6, 2020. The copyright holder for this preprint (which was not certified by peer review) is the author/funder. All rights reserved. No reuse allowed without permission.

715 composition can be approximately mimicked with reference strains (Fig. I,K),
716 incorporating genetically modifiable organisms and existing mutant libraries in our
717 SICs could open additional applications.
718
719 A remarkable aspect of our SICs is their ability to recapitulate *in vivo* behaviors.
720 Community composition was generally maintained through passaging in BHI (Fig. 1,7)
721 and the microbial metaproteomic signature was similar between feces and SICs (Fig.
722 S1E), suggesting that many interspecies interactions are conserved in this medium.
723 Moreover, SICs derived from mice during and after antibiotic treatment were more
724 susceptible to invasion by *S*. Typhimurium than SICs derived before treatment (Fig. 6A-
725 C). While previous studies reported that ciprofloxacin treatment can increase the
726 colonization susceptibility of chemostat-grown microbial communities (Carman et al.,
727 2004), our experiments were conducted in the absence of ciprofloxacin at the time of
728 challenge. Thus, the compositional changes elicited by antibiotics *in vivo* are maintained
729 *in vitro*, leading to different functional outcomes.
730
731 Importantly, our study also allowed a quantitative comparison between the antibiotic
732 response of the gut microbiota *in vivo* and *in vitro* (Fig. 5), which revealed remarkable
733 similarities in taxon-specific changes in diversity (Fig. 5H). Many aspects of the
734 recovery dynamics that are confounded by multiple factors *in vivo* were clarified by our

bioRxiv preprint doi: https://doi.org/10.1101/2020.07.06.190181; this version posted July 6, 2020. The copyright holder for this preprint (which was not certified by peer review) is the author/funder. All rights reserved. No reuse allowed without permission.

735 *in vitro* studies. The lack of substantial recovery in richness *in vitro* after ciprofloxacin
736 treatment (Fig. 5D) suggests that the ~4-fold increase *in vivo* post-treatment relative to
737 residual samples (Fig. S1B) comes from environmental reseeding or increased densities
738 *in vivo*. Notably, SICs derived from feces at the peak or during residual treatment were
739 more similar to their inocula than to feces post-treatment (Fig. 2A), indicating that
740 removal of the drug in inoculating media *in vitro* is not enough to recover taxa that
741 went undetectable *in vivo*. Highlighting the physiological relevance of such reservoirs,
742 our *in vivo* studies indicate that singly housed mice experience a prolonged decrease in
743 viable load, *Bacteroides* abundance, and diversity compared with co-housed mice during
744 antibiotic treatment, with highly heterogeneous recovery dynamics across mice (Ng et
745 al., 2019). Disruption of community composition and the set of species that become
746 undetectable are mostly deterministic (Fig. S9C,H). Our findings show that the recovery
747 of some species such as *B. fragilis* from undetectable levels across multiple passages
748 does not require environmental reservoirs (e.g. via coprophagy in mice) or larger
749 population sizes *in vivo*, indicating that resilience is built-in to some species, and
750 pointing to SICs enabling the elucidation of aspects of community ecology that can be
751 uncoupled from host dependence. Future work with fecal-derived SICs, including
752 comparisons of our methodology with other fecal-derived and bottom-up reconstitution
753 approaches (Macfarlane et al., 1998; Minekus et al., 1999; Van de Wiele et al., 2015),

bioRxiv preprint doi: https://doi.org/10.1101/2020.07.06.190181; this version posted July 6, 2020. The copyright holder for this preprint (which was not certified by peer review) is the author/funder. All rights reserved. No reuse allowed without permission.

754 should elucidate the interplay among antibiotic sensitivity and tolerance, duration, and
755 strength of antibiotic exposure, and migration between hosts and the environment.

756

757 In general, top-down and bottom-up SICs serve as powerful, complementary resources
758 for the microbiota field. Bottom-up SICs can be used to measure interspecies
759 interactions using drop-out experiments (Gutierrez and Garrido, 2019), while top-down
760 SICs provide a more complex template for evaluating the effects of perturbations and
761 comparing to *in vivo* results, including the potential for blooming of species from below
762 the limit of detection pre-treatment. The overrepresentation of fast-growing species in
763 SICs (Fig. 1) and their receding in SIC-colonized mice (Fig. S1C,D) shed light on the
764 bacterial taxa whose growth is controlled by the host. Further, we predicted the effects
765 of ciprofloxacin (Fig. 4G) at the ASV level through isolate-sensitivity measurements and
766 perturbations to pre-treatment SICs. The emergence of resistant strains, and their out-
767 competition by close relatives, can also be predicted (Fig. 6). The observed correlation
768 between changes upon ciprofloxacin treatment and strain sensitivities (Fig. 4F) suggests
769 that interspecies interactions are not a strong modifier of antibiotic responses in these
770 SICs. Nonetheless, interspecies interactions can change antibiotic sensitivity in
771 auxotrophic food-webs (Adamowicz et al., 2018) and induce tolerance (Aranda-Díaz et
772 al., 2019). Notably, we can only measure isolate sensitivities in the culturable portion of
773 the SICs (Fig. 3B), and metabolic dependencies of the strains we did not isolate could

bioRxiv preprint doi: https://doi.org/10.1101/2020.07.06.190181; this version posted July 6, 2020. The copyright holder for this preprint (which was not certified by peer review) is the author/funder. All rights reserved. No reuse allowed without permission.

774 affect their survival. Further work will be needed to investigate the role of tolerance in
775 the ability of specific taxa to recover after treatment (Fig. 5F,K). These findings suggest
776 that first dissecting *in vitro* how a gut community is remodeled by a perturbation can
777 serve as a powerful pre-screening tool before expensive mouse experiments.
778
779 Many other fascinating questions should be tackled in the future using our *in vitro*
780 approach, which can be scaled to thousands of SICs simultaneously. Since a fecal
781 sample from a mammalian host likely represents an average over the spatial
782 localization and physiologies determined by the history and environmental contexts
783 within the gut, a similar culturomics approach should be applied to samples from other
784 locations in the gastrointestinal tract. Our observation that BHI-passaged SICs can shift
785 the host proteome of germ-free mice toward that of humanized mice (Fig. S1D) suggests
786 that SICs can also be safely re-introduced to their original hosts. Fecal microbiota
787 transplantation is a promising therapy for diseases like *Clostridium difficile* infection
788 (Drekonja et al., 2015) and aids in recovery after chemotherapy (Le Bastard et al., 2018),
789 diarrhea (Tropini et al., 2018), and antibiotic treatments (Ng et al., 2019). However, the
790 lack of standardization and danger due to potential collateral infections are major
791 barriers for the wide therapeutic use of fecal microbiota transplantation (Cammarota et
792 al., 2017). SICs may lower the risk of infection and improve manufacturing efficiency
793 (Khoruts and Weingarden, 2014), thus overcoming these barriers to therapy. More

bioRxiv preprint doi: https://doi.org/10.1101/2020.07.06.190181; this version posted July 6, 2020. The copyright holder for this preprint (which was not certified by peer review) is the author/funder. All rights reserved. No reuse allowed without permission.

794 generally, SICs should bridge mechanistic studies of microbial ecology and human-

795 relevant *in vivo* systems to accelerate the pace of discovery in the microbiota field.

bioRxiv preprint doi: https://doi.org/10.1101/2020.07.06.190181; this version posted July 6, 2020. The copyright holder for this preprint (which was not certified by peer review) is the author/funder. All rights reserved. No reuse allowed without permission.

Author Contributions

A.A.-D, K.M.N., J.L.S., and K.C.H designed the research; A.A.-D., K.M.N., T.T., S.D., F.B.Y., I.R.R., T.C., S.H, K.V., C.G.G., and T.N. performed the research; A.A.-D., K.M.N., D.D., and C.G.G. analyzed the data; and A.A.-D, J.L.S., and K.C.H wrote the paper and all authors reviewed it before submission.

Acknowledgments

The authors thank Rebecca Culver, Carolina Tropini, Kali Pruss, Alice Cheng, Manohary Rajendram, Surya Tripathi, and Myles Bartholomew for technical assistance; and Rita Oliveira, Lisa Willis, Handuo Shi, and Po-Yi Ho for valuable comments on the manuscript. Some reference strains used in this study were kindly provided by Michael Fischbach and Denise Monack. A.A.-D. is a Howard Hughes Medical Institute International Student Research fellow, a Stanford Bio-X Bowes fellow, and a Siebel Scholar. The authors acknowledge funding from the Allen Discovery Center at Stanford on Systems Modeling of Infection (to K.M.N. and K.C.H.). J.L.S. and K.C.H. are Chan Zuckerberg Investigators.

bioRxiv preprint doi: https://doi.org/10.1101/2020.07.06.190181; this version posted July 6, 2020. The copyright holder for this preprint (which was not certified by peer review) is the author/funder. All rights reserved. No reuse allowed without permission.

812 **Methods**

813

814 *Mouse sampling*

815 All mouse experiments were conducted in accordance with the Administrative Panel on
816 Laboratory Animal Care, Stanford University's IACUC. Germ-free, female,Swiss-
817 Webster mice were gavaged with a human fecal sample obtained from a healthy
818 anonymous donor as previously described (Kashyap et al., 2013). The microbiota was
819 allowed to equilibrate for 6-8 weeks before perturbation experiments commenced.
820 Humanized mice were orally gavaged with antibiotics (Sigma Aldrich) dissolved in 200
821 μL water for 5 days. For experiments involving a dietary switch, mice were first fed a
822 standard diet (Purina LabDiet 5010) rich in MACs, and then a defined low-MAC diet
823 (Harlan TD.86489) in which the sole carbohydrates are sucrose (31% w/w), cornstarch
824 (31% w/w), and cellulose (5% w/w). Mice were euthanized with CO_2, and death was
825 confirmed via cervical dislocation.

826

827 Fecal pellets were sampled on ice and taken into an anaerobic chamber within 30 min.
828 Human stool samples were collected from 3 healthy donors by scooping a small sample
829 from a receptacle into a conical tube on ice. The samples were transferred to an
830 anaerobic chamber within 5 min of sampling.

831

bioRxiv preprint doi: https://doi.org/10.1101/2020.07.06.190181; this version posted July 6, 2020. The copyright holder for this preprint (which was not certified by peer review) is the author/funder. All rights reserved. No reuse allowed without permission.

832 ***SIC passaging, storage, and revival***

833 Approximately 100 mg of stool samples from humanized mice or human donors were
834 resuspended into 200 μL phosphate-buffered saline (PBS) in 1.5 mL microcentrifuge
835 tubes. Samples were incubated in PBS for 10-15 min at room temperature to encourage
836 large pieces of fecal matter to disintegrate. Samples were vortexed for 5 min and
837 allowed to sit for 1 min to let food particles settle. One microliter of this resuspension
838 was inoculated into 200 μL medium in 96-well polystyrene microplates (Greiner Bio-
839 One). Each resuspension was inoculated into four media (Table S2) in triplicate. The
840 plate was covered with optical film, with a small (~0.5 mm) hole poked above each well,
841 outside of the plate reader's light path, to allow gas exchange.

842

843 Incubation and optical density (OD) measurements were performed with an Epoch 2
844 plate reader (BioTek) in an anaerobic chamber at 37 °C with continuous shaking and
845 OD_{600} measured at 7.5-min intervals. Plates were incubated in the plate reader for 48 h
846 and then 1 μL of this saturated culture was transferred into 200 μL of fresh medium in a
847 new plate. We refer to a 48-h cycle from inoculation to saturation as one passage.
848 Samples used in the passaging experiments in Figs. 1 and 2 were taken in consecutive
849 days, hence the plate was removed from the plate reader every 24 h, to inoculate and/or
850 passage corresponding SICs. On a given day, if the communities were not passaged,

bioRxiv preprint doi: https://doi.org/10.1101/2020.07.06.190181; this version posted July 6, 2020. The copyright holder for this preprint (which was not certified by peer review) is the author/funder. All rights reserved. No reuse allowed without permission.

851 then the whole volume was transferred into a new plate.

852

853 After passaging, 50 μL of the cultures were mixed with 50 μL sterile 50% glycerol (v/v
854 in water) in crimp vials, sealed, and stored at -80 °C for long-term storage. The
855 remaining volume was stored in the 96-well plate at -80 °C with an aluminum seal until
856 DNA was extracted. BHI SICs were revived for experimentation by inoculation of
857 frozen glycerol stocks directly into 3 mL BHI. Revived communities were incubated at
858 37 °C for 48 h and passaged twice before experimentation by diluting 1:200 into fresh
859 medium every 48 h.

860

861 ***SIC colonization***

862 Mice were humanized with a human fecal sample obtained from the same healthy
863 anonymous donor as was used for the ciprofloxacin-treatment experiment (Fig. 1A).
864 Four weeks after humanization, fecal pellets were collected from 11 mice housed across
865 3 cages. A mixture of the 11 fecal pellets was used to inoculate 3 mL BHI to derive an
866 SIC as described above. The SIC was passaged every 48 h with a 1:200 dilution into
867 fresh medium. After 5 passages, a frozen stock was made by mixing equal volumes of a
868 saturated culture and 50% glycerol (v/v in water). The SIC was revived by inoculating
869 the frozen stock into 3 mL BHI and passaging twice before using 200 μL of the saturated
870 culture to gavage germ-free, female, Swiss-Webster mice. culture. Fecal pellets were

bioRxiv preprint doi: https://doi.org/10.1101/2020.07.06.190181; this version posted July 6, 2020. The copyright holder for this preprint (which was not certified by peer review) is the author/funder. All rights reserved. No reuse allowed without permission.

sampled from the germ-free mice on the day that they were gavaged, on day 24 after colonization for proteome analysis, and on day 28 for 16S sequencing.

Strains and growth media

Growth media are listed in Table S2. These media were chosen because of their ability to grow diverse microbes: the nutrient-rich Brain Heart Infusion (BHI) is widely used to culture fastidious microorganisms; Tryptone-Yeast extract-Glucose (TYG), which is often used to culture members of the *Bacteroides* genus that includes many prevalent human commensals; Gifu Anaerobic Medium (GAM; a mixture of animal, plant, and yeast digests and extracts supplemented with glucose and starch), which cultures individual species with relative yields similar to their abundances in human microbiotas (Rettedal et al., 2014); and Yeast extract, Casitone, and Fatty Acids (YCFA), which has been used to culture a wide range of human gut commensals (Browne et al., 2016). Isolated and reference strains are listed in Tables S1 and S3, respectively. All media and materials were made anaerobic by incubating in a custom anerobic chamber (Coy Labs) for 48 h before use.

Growth analyses

Maximal growth rate was calculated as the maximal slope of ln(OD) with respect to time (calculated from a linear regression of a sliding window of 11 timepoints). The

bioRxiv preprint doi: https://doi.org/10.1101/2020.07.06.190181; this version posted July 6, 2020. The copyright holder for this preprint (which was not certified by peer review) is the author/funder. All rights reserved. No reuse allowed without permission.

duration of lag phase was defined as the time at which a strain first reached its half-maximum growth rate.

16S rRNA sequencing

DNA was extracted from whole fecal pellets or 50 µL of culture with a DNeasy PowerSoil HTP 96 kit (Qiagen 12955-4). 16S rRNA amplicons were generated using Earth Microbiome Project-recommended 515F/806R primer pairs using the 5PRIME HotMasterMix (Quantabio 2200410) with the following program in a thermocycler: 94 °C for 3 min, 35 cycles of 94 °C for 45 s, 50 °C for 60 s, and 72 °C for 90 s, followed by 72 °C for 10 min. PCR products were cleaned, quantified, and pooled using the UltraClean 96 PCR Cleanup kit (Qiagen 12596-4) and Quant-iT dsDNA High Sensitivity Assay kit (Invitrogen Q33120). Samples were sequenced with 250- or 300-bp reads on a MiSeq (Illumina).

Samples were de-multiplexed with Qiime v. 1.9.1 (Caporaso et al., 2010) using the commands "split_libraries_fastq.py --rev_comp_mapping_barcodes --rev_comp_barcode --store_demultiplexed_fastq --max_bad_run_length 999 --min_per_read_length_fraction .01 --sequence_max_n 999 --phred_quality_threshold 0" and "split_sequence_file_on_sample_ids.py". Subsequent processing was performed using DADA2 as previously described (Callahan et al., 2016). truncLenF and truncLenR

bioRxiv preprint doi: https://doi.org/10.1101/2020.07.06.190181; this version posted July 6, 2020. The copyright holder for this preprint (which was not certified by peer review) is the author/funder. All rights reserved. No reuse allowed without permission.

911 parameters were set to 240 and 180, respectively. Resulting ASV sequences were
912 assigned taxonomy with Qiime, using the commands "assign_taxonomy.py",
913 "align_seqs.py", and "make_philogeny.py". Custom MATLAB R2018a (MathWorks)
914 scripts were used for further analysis.
915
916 ASVs were classified as contaminants and removed from further analysis if they
917 appeared with significantly higher relative abundances (p<0.001, t-test) in control
918 samples (water added to DNA extraction step).
919
920 Alpha diversity (richness) was measured by rarefying all samples to 5000 reads and
921 calculating the number of taxa with relative abundance >0. Shannon diversity was
922 calculated using $S = \sum_{i=1}^{N} -p_i \ln p_i$, where p is the relative abundance of the ith taxon
923 and N is the total number of taxa with p>0. Evenness was calculated using the Pielou
924 index by normalizing Shannon diversity by the maximum Shannon index for the
925 number of taxa: $J = {S}/{\ln N}$.
926
927 Weighted and unweighted Unifrac distances between samples for beta diversity were
928 calculated using custom MATLAB code. Unifrac was calculated as described in
929 (Lozupone and Knight, 2005). Weighted Unifrac was calculated as described in
930 (Lozupone et al., 2007): for samples A and B, $u_w = \sum_i^n b_i \times |A_i - B_i|$, where n is the total

bioRxiv preprint doi: https://doi.org/10.1101/2020.07.06.190181; this version posted July 6, 2020. The copyright holder for this preprint (which was not certified by peer review) is the author/funder. All rights reserved. No reuse allowed without permission.

number of branches in the tree, b_i is the length of branch i, and A_i and B_i are the relative abundances of the taxa that descend from branch i in samples A and B, respectively. No further normalization was performed. Only taxa present at >0.01% in more than two samples were used to calculate distances. Principal coordinate analyses were performed on unweighted Unifrac distances between samples with >5000 reads.

Isolation of strains

SICs were resuspended in PBS and plated onto BHI, BHI-S, or GAM plates. Plates were incubated at 37 °C in an anaerobic chamber. After 2 days, colonies were grown in the medium corresponding to the plate from which they were isolated for 2 days, and glycerol stocked. Strains were identified via high-throughput MALDI-TOF mass spectrometry of whole colonies, and subsequent matching of spectra to a reference library with a MALDI Biotyper System (Bruker), following manufacturer's instructions and including formic acid lysis. For the SIC that we attempted to reconstitute, 15 distinct strains were obtained and their taxonomy was checked by Sanger sequencing. Genomic DNA was extracted from pure cultures using a DNeasy UltraClean 96 Microbial Kit (Qiagen 10196-4) or DNeasy Blood and Tissue Kit (Qiagen 69504) kit. The 16S gene was amplified using primers 5'AGAGTTTGATCCTGGCTCAG and 5'GACGGGCGGTGWGTRCA, and the amplicon was Sanger sequenced. Taxonomic

bioRxiv preprint doi: https://doi.org/10.1101/2020.07.06.190181; this version posted July 6, 2020. The copyright holder for this preprint (which was not certified by peer review) is the author/funder. All rights reserved. No reuse allowed without permission.

assignment was performed by alignment using BLAST against the 16S ribosomal RNA sequences (Bacterial and Archaea) database.

Community reconstitution

For community reconstitution, frozen stocks of isolated (Table S1) or reference (Table S3) strains were streaked onto BHI 5% sheep blood agar plates and incubated for 48 h at 37 °C in anaerobic conditions. A single colony of each strain was inoculated into 3 mL BHI in isolation, and incubated for 48 h at 37 °C. OD was measured for each strain and all were diluted to a final OD of 1×10^{-4} before mixing in 200 µL BHI in a 96-well plate. Mixed cultures were grown for 48 h in a plate reader to measure growth. After 48 h the cultures were diluted 1:200 into fresh BHI.

Antibiotic sensitivity estimation

Frozen stocks of isolated strains (Table S1) were streaked onto BHI 5% sheep blood agar plates and incubated for 48 h at 37 °C in anaerobic conditions. A single colony of each strain was inoculated into a 3 mL monoculture in BHI, and incubated for 48 h at 37 °C. Cultures were then diluted 1:200 into fresh BHI containing 0.5-32 µg/mL ciprofloxacin. The minimum inhibitory concentration (MIC) for each strain was calculated as the minimum dose necessary to completely inhibit growth as measured by OD after 48 h of incubation.

bioRxiv preprint doi: https://doi.org/10.1101/2020.07.06.190181; this version posted July 6, 2020. The copyright holder for this preprint (which was not certified by peer review) is the author/funder. All rights reserved. No reuse allowed without permission.

970

971 **In vitro *antibiotic treatment***

972 SICs were revived in 3 mL BHI and passaged twice before experimentation by diluting
973 15 µL into 3 mL fresh medium every 48 h. One microliter of the SICs was then diluted
974 into 200 µL fresh BHI containing 0.5-32 µg/mL ciprofloxacin. Growth was measured in
975 a plate reader as described above, and 48 h-old cultures were stored at -80 °C until DNA
976 was extracted.

977

978 **In vitro S. *Typhimurium challenge***

979 SICs were revived in 200 µL BHI in microplates and passaged twice by diluting 1 µL
980 into 200 µL fresh medium every 48 h. A frozen stock of *S*. Typhimurium strain SL1344
981 was grown anaerobically at 37 °C for 24 h in BHI. One microliter of the SICs and 1 µL of
982 *S*. Typhimurium adjusted to OD_{600}=0.1 was diluted into 200 µL fresh BHI. Saturated co-
983 cultures were serially diluted into sterile PBS after 48 h of incubation at 37 °C. Three
984 microliters of a $1:10^4$ dilution were spotted onto LB agar with 50 µg/mL streptomycin to
985 select for *S*. Typhimurium. Pictures of colonies (Fig. 6B, S8A) were taken after 48 h of
986 incubation at 37 °C in aerobic conditions.

987

988 For single-cell quantification of *S*. Typhimurium levels, we followed the protocol
989 described above to grow SICs and an *S*. typhimurium 14028s strain expressing

bioRxiv preprint doi: https://doi.org/10.1101/2020.07.06.190181; this version posted July 6, 2020. The copyright holder for this preprint (which was not certified by peer review) is the author/funder. All rights reserved. No reuse allowed without permission.

cytoplasmic mCherry (Table S3) prior to co-culturing. SICs and *S*. Typhimurium were mixed at various ratios and incubated anaerobically for 48 h at 37 °C. Saturated cultures were removed from the anaerobic chamber and spotted onto PBS agar plates to perform high-throughput phase and fluorescence microscopy (Shi et al., 2017). Percentages of *S*. Typhimurium (Fig. 6C, S8B) were estimated by calculating the proportion of pixels within cell contours segmented from phase images whose fluorescence was above a threshold that clearly separated mCherry-positive and mCherry-negative cells using custom Matlab code.

Isolation of stool proteins and peptides

Isolation of stool proteins broadly followed the protocol in (Gonzalez et al., 2020). Briefly, ~50 mg mouse pellets or pelleted cells from 1 mL saturated cultures were aliquoted into a 96-well plate along with ~600 mg of 0.1-mm ceramic beads (Omni International, #27-6006). To each well, 750 µL lysis buffer (6 M urea, 5% sodium dodecyl sulfate, and 50 mM Tris, pH 8.1) was added and plates were sealed with sealing mats (Omni International, #27-530). Sealed plates were subjected to 10 min of bead beating at 20 Hz using a Qiagen Tissuelyser II. After bead beating, each plate was centrifuged at 3000 rcf at 4 °C for 10 min. Five hundred microliters of the resulting supernatant were transferred to a new 2-mL 96-well plate (Waters, 186002482), sealed with a sealing mat, spun again at 3000 rcf at 4 °C for 10 min, then transferred to a fresh 2-mL plate. Samples

bioRxiv preprint doi: https://doi.org/10.1101/2020.07.06.190181; this version posted July 6, 2020. The copyright holder for this preprint (which was not certified by peer review) is the author/funder. All rights reserved. No reuse allowed without permission.

were reduced with 10 µL of 500 mM dithiothreitol (Sigma-Aldrich) for 30 min at 47 °C and alkylated with 30 µL of 500 mM iodoacetamide (Sigma-Aldrich) for 1 h at room temperature in the dark. Fifty microliters of the reduced and alkylated supernatant were transferred to a new 2-mL 96-well plate for further processing, while the remaining material was stored at -80 °C.

Supernatant-resident stool proteins were washed, digested, and eluted as described in the Protifi S-trap protocol (http://www.protifi.com/wp-content/uploads/2018/08/S-Trap-96-well-plate-long-1.4.pdf). Briefly, the 50 µL supernatant was acidified with 5 µL of 12% phosphoric acid to which 300 µL S-trap binding buffer was added. Each resulting mixture was loaded into a single well. Positive pressure was used to load the proteins into each well with a Positive Pressure-96 Processor (Waters) with pressure set at 6-9 psi on the "Low-Flow" setting. Loaded proteins were washed with 300 µL Binding Buffer (90% methanol and 10% triethylammonium bicarbonate buffer (TEAB, Sigma-Aldrich, #T7408), adjusted to pH 7.1 using phosphoric acid) five times. After washing, 125 µL digestion buffer (100 mM TEAB and 5 µg trypsin) were added and proteins were digested for 3 h at 47 °C. Peptides were eluted with 100 µL TEAB, followed by 100 µL of 0.2% formic acid, followed by 100 µL of 50% acetonitrile, 0.2% formic acid. These peptides were captured in a 1-mL 96-well plate (Thermo Scientific, #AB-1127) and the volume was dried down in a Centrivap speedvac (Model 7810016). Plated samples were

bioRxiv preprint doi: https://doi.org/10.1101/2020.07.06.190181; this version posted July 6, 2020. The copyright holder for this preprint (which was not certified by peer review) is the author/funder. All rights reserved. No reuse allowed without permission.

desalted using RP-S cartridges on an Agilent Bravo AssayMAP using the built-in desalting protocol, eluted with 50% acetontrile, and dried down. Plated peptide concentrations were normalized using a Nanodrop ND-1000.

Mass spectrometry

Peptide samples were diluted to 0.5 μg/μL. Subsequently, 1 μL was loaded onto an in-house, laser-pulled 100-μm inner diameter nanospray column packed to ~220 mm with 3-μm 2A C18 beads (Reprosil). Peptides were separated by reversed-phase chromatography on a Dionex Ultimate 3000 HPLC. Buffer A of the mobile phase contained 0.1% formic acid in HPLC-grade water, and buffer B contained 0.1% formic acid in acetonitrile. An initial 2-min isocratic gradient flowing 3% B was followed by a linear increase to 25% B for 115 min, then increased to 45% B over 15 min, and a final increase to 95% B over 15 min, whereupon B was held for 6 min and returned back to baseline in 2 min and held for 10 min, for a total of 183 min. The HPLC flow rate was 0.400 μL/min. Samples were run on a Thermo Fusion Lumos mass spectrometer that collected mass spectrometry data in positive-ion mode within the 400-1500 m/z range with an initial Orbitrap scan resolution of 120,000, followed by high-energy collision-induced dissociation and analysis in the orbitrap using "Top Speed" dynamic identification with dynamic exclusion enabled (repeat count of 1, exclusion duration of

bioRxiv preprint doi: https://doi.org/10.1101/2020.07.06.190181; this version posted July 6, 2020. The copyright holder for this preprint (which was not certified by peer review) is the author/funder. All rights reserved. No reuse allowed without permission.

90 s). The automatic gain control was set to 4e5 for FT full mass spectrometry and to 1e4 for ITMSn.

Peptide/protein database searching

Mass spectra were searched using Proteome Discoverer 2.2 using the built-in SEQUEST search algorithm. Three FASTA databases were searched: Uniprot Swiss-Prot *Mus musculus* (taxon ID 10090, downloaded January 2017), a custom concatenated database containing proteome data for all 15 bacteria in the reconstituted SIC (Fig. 3B), and a database containing common preparatory contaminants. Target-decoy searching at both the peptide and protein level was employed with a strict false discovery-rate cutoff of 0.05 using the Percolator algorithm built into Proteome Discoverer 2.2. Enzyme specificity was set to tryptic, with static peptide modifications set to cambamidomethylation (+57.0214 Da). Dynamic modifications were set to oxidation (+15.995 Da) and N-terminal protein acetylation (+42.011 Da). Only high-confidence proteins ($q < 0.01$) were used for analysis.

Proteome analysis

Custom MATLAB R2018a (MathWorks) scripts were used to analyze protein abundances. *M. musculus* analyses were restricted to proteins that were 10 times more abundant in germ-free, humanized, or SIC-colonized mice samples than in any *in vitro*

bioRxiv preprint doi: https://doi.org/10.1101/2020.07.06.190181; this version posted July 6, 2020. The copyright holder for this preprint (which was not certified by peer review) is the author/funder. All rights reserved. No reuse allowed without permission.

bacterial cultures in our dataset. Similarly, *B. fragilis* and *B. producta* proteome analyses were restricted to proteins that were 10 times more abundant in humanized mice, SIC-colonized mice, and SIC samples than in germ-free mice.

bioRxiv preprint doi: https://doi.org/10.1101/2020.07.06.190181; this version posted July 6, 2020. The copyright holder for this preprint (which was not certified by peer review) is the author/funder. All rights reserved. No reuse allowed without permission.

Figure Legends

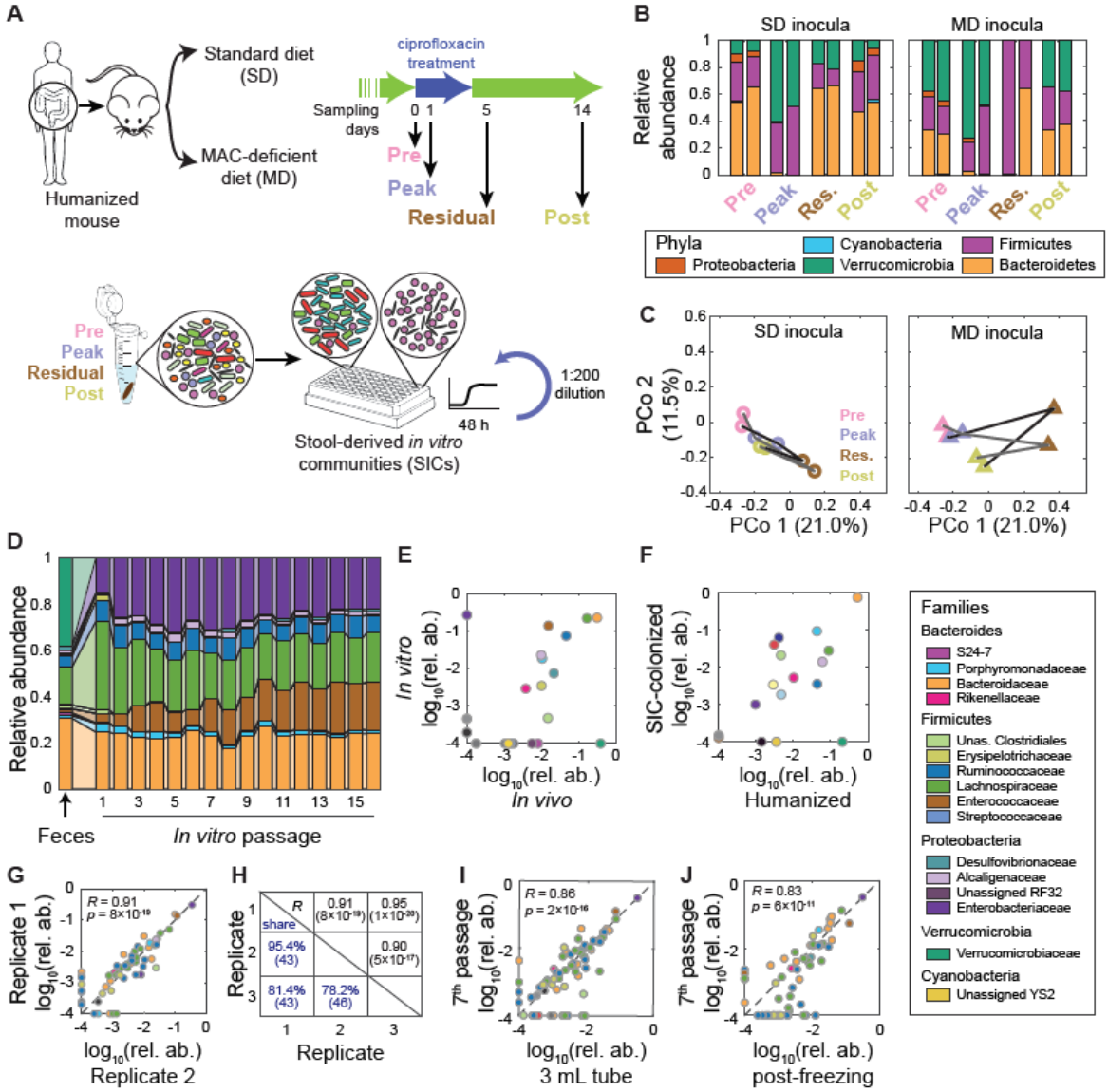

Figure 1: High-throughput cultivation of feces from humanized mice yields stable, complex and reproducible microbial communities.

A) Experimental setup. Germ-free mice colonized with feces from a single human donor ("humanized") were fed a SD or an MD and treated with ciprofloxacin for 5 days. Inocula from two mice on each diet were taken on four days (0, 1, 5, 14)

bioRxiv preprint doi: https://doi.org/10.1101/2020.07.06.190181; this version posted July 6, 2020. The copyright holder for this preprint (which was not certified by peer review) is the author/funder. All rights reserved. No reuse allowed without permission.

before, during, and after treatment, and were inoculated into anaerobic batch culture and passaged with dilution every 48 h to derive SICs. Sixteen samples (2 diets, 2 mice, 4 time points during ciprofloxacin treatment) were inoculated into 4 media (BHI, TYG, GAM, and YCFA) in triplicate.

B) Ciprofloxacin elicits large changes in microbiota composition at the phylum level *in vivo*. Each time point has two bars corresponding to the two mice in each group.

C) Diet alters the trajectory of microbiota reorganization during ciprofloxacin treatment *in vivo*. PCoA of community composition of the fecal inocula in (B) using unweighted Unifrac distance computed on all *in vivo* and *in vitro* samples at the ASV level.

D) *In vitro* passaging produces stable and complex SICs. Family-level compositions of an example SIC derived from the fecal inoculum of pre-treatment MD mouse 1 during 16 rounds of *in vitro* passaging in BHI.

E) *In vitro* passaging can produce an SIC that resembles the fecal inoculum. Mean family-level $\log_{10}$(relative abundance) of passages 4-16 for the SIC in (D) and the fecal inoculum from which it originated. Families with relative abundance of 0 were set to 10^{-4} for visualization.

F) Colonization of germ-free mice with an SIC restores families overrepresented *in vitro* back to levels similar to those in the humanized mice from which the SIC

bioRxiv preprint doi: https://doi.org/10.1101/2020.07.06.190181; this version posted July 6, 2020. The copyright holder for this preprint (which was not certified by peer review) is the author/funder. All rights reserved. No reuse allowed without permission.

was derived. Comparison of the family-level $\log_{10}$(relative abundance) of a humanized-mouse fecal inoculum and the mean family-level $\log_{10}$(relative abundance) of ex-germ-free mice colonized with an SIC derived from the humanized-mouse fecal inoculum (inoculum n=1, SIC-colonized n=3). Families with relative abundance of 0 were set to 10^{-4} for visualization.

G,H) *In vitro*-passaged SICs are highly reproducible. (G) ASV-level $\log_{10}$(relative abundance) for two technical replicates of the SIC in (D) after 7 passages. ASVs with relative abundance of 0 were set to 10^{-4} for visualization. (H) Summary of the reproducibility of the three replicates for the SIC in (D). R and p were computed using only ASVs present in both samples. Also shown is the percentage of ASVs that are present in both replicates at >0.1% abundance ("shared"), with the total number of ASVs in parenthesis.

I,J) SICs can be grown in larger volumes and can be frozen and revived without affecting composition. ASV-level $\log_{10}$(relative abundance) values for the SIC in (D) after 7 passages were compared with the same SIC grown for one passage in a larger vessel without shaking (I), and after freezing with 25% glycerol at -80 °C and reviving for one passage (J). R and p were computed using only ASVs present in both samples. ASVs with relative abundance of zero were set to 10^{-4} for visualization.

bioRxiv preprint doi: https://doi.org/10.1101/2020.07.06.190181; this version posted July 6, 2020. The copyright holder for this preprint (which was not certified by peer review) is the author/funder. All rights reserved. No reuse allowed without permission.

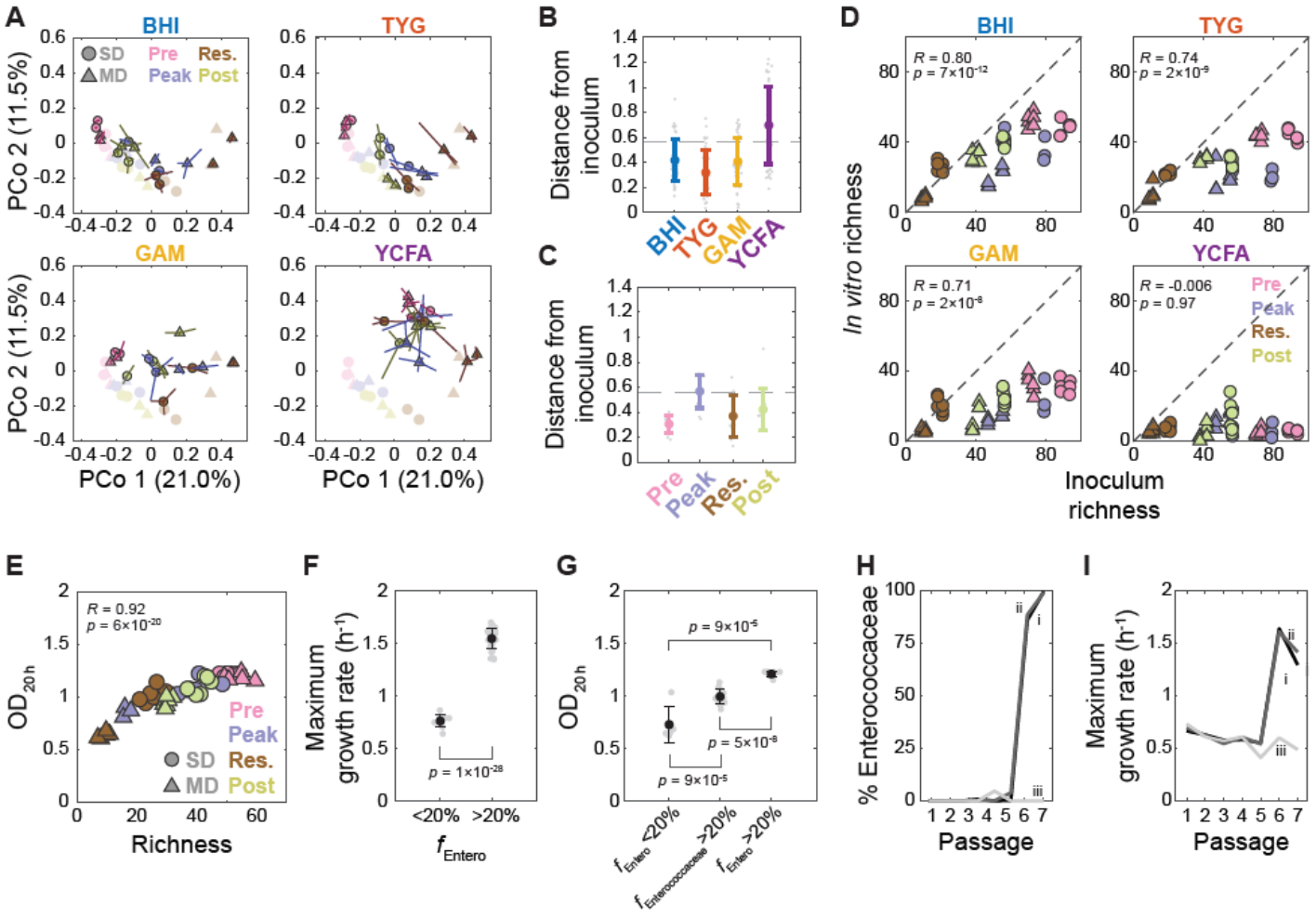

Figure 2: SIC composition is determined by inoculum and media, and is predictive of yield and growth rate.

A) Medium and inoculum determine the final composition of passaged SICs. The 7th passage of all 192 SICs in a PCoA of SIC composition using unweighted Unifrac distance computed on all *in vivo* and *in vitro* samples at the ASV level. Samples are separated by media, with colors and shapes representing the timepoint during ciprofloxacin treatment and diet, respectively, in the mice from which the inocula were taken. Symbols are the centroid of three replicates, with lines

bioRxiv preprint doi: https://doi.org/10.1101/2020.07.06.190181; this version posted July 6, 2020. The copyright holder for this preprint (which was not certified by peer review) is the author/funder. All rights reserved. No reuse allowed without permission.

connecting the replicates to the centroid. Original fecal inocula are plotted in light colors (same data as in Fig. 1C).

B) Most steady-state SICs are similar to the fecal samples from which they were derived. Weighted Unifrac distance of the 7th passage of each SIC to the corresponding fecal inoculum. Colored circles, mean distance for each medium; individual SICs in gray. Error bars, standard deviations (SD); *n*=48. Dashed line, mean distance between fecal samples.

C) SICs derived from feces at the peak of treatment *in vivo* are most distinct from the composition of their inoculum. Weighted Unifrac distance of the 7th passage in BHI of each SIC to their fecal inoculum. Symbols and line are as in (B); *n*=12.

D) SIC diversity correlates with inoculum diversity in most media. Richness (number of ASVs in rarefied data) was compared for the 7th passage of each SIC and the corresponding fecal inocula and separated and colored/shaped as in (A). *R* and *p* were calculated from all samples in a given medium; *n*=48.

E) SIC yield scales with diversity. Mean OD of SICs after 20 h of growth in BHI passages 3-7 increases with increasing richness (number of ASVs in rarefied data) in passage 7. *R*, Pearson correlation coefficient; *n*=48.

F) Maximum growth rate is correlated with the abundance of fast-growing families. Maximum growth rate was calculated from growth curves during the 7th passage and BHI-passaged SICs were classified based on the relative abundance of

bioRxiv preprint doi: https://doi.org/10.1101/2020.07.06.190181; this version posted July 6, 2020. The copyright holder for this preprint (which was not certified by peer review) is the author/funder. All rights reserved. No reuse allowed without permission.

Enterobacteriaceae and Enterococcaceae (f_{Entero}). Black circles, mean maximum growth rate for each group (n=11 for $f_{\text{Entero}} < 20\%$ and n=37 for $f_{\text{Entero}} > 20\%$); error bars, SD. Individual data points are plotted in gray. p-value is from a Student's two-sided t-test between the two groups.

G) SIC yield scales with the presence of fast-growing families. $OD_{20\,h}$ is as in (E). SICs with >20% Enterococcaceae but <20% Enterobacteriaceae are labeled as $f_{Enterococcaceae}$>20%. Black circles, mean maximum growth rate for each group (n=5 for $f_{\text{Entero}} < 20\%$, n=15 for $f_{Enterococcaceae}$>20%, and n=8 for $f_{\text{Entero}} > 20\%$); error bars, SD. Individual data points are plotted in gray. p-values are from a Student's two-sided t-test between each pairwise comparison.

H-I) Changes in SIC composition during passaging are reflected in altered SIC growth. Percentage of Enterococcaceae (H) and maximum growth rate (I) for three technical replicates (i-iii) of the SIC derived from SD mouse 2 during residual treatment passaged in YCFA. The increase in maximum growth rate and blooming of the Enterococcaceae occur concurrently in two of the replicates.

bioRxiv preprint doi: https://doi.org/10.1101/2020.07.06.190181; this version posted July 6, 2020. The copyright holder for this preprint (which was not certified by peer review) is the author/funder. All rights reserved. No reuse allowed without permission.

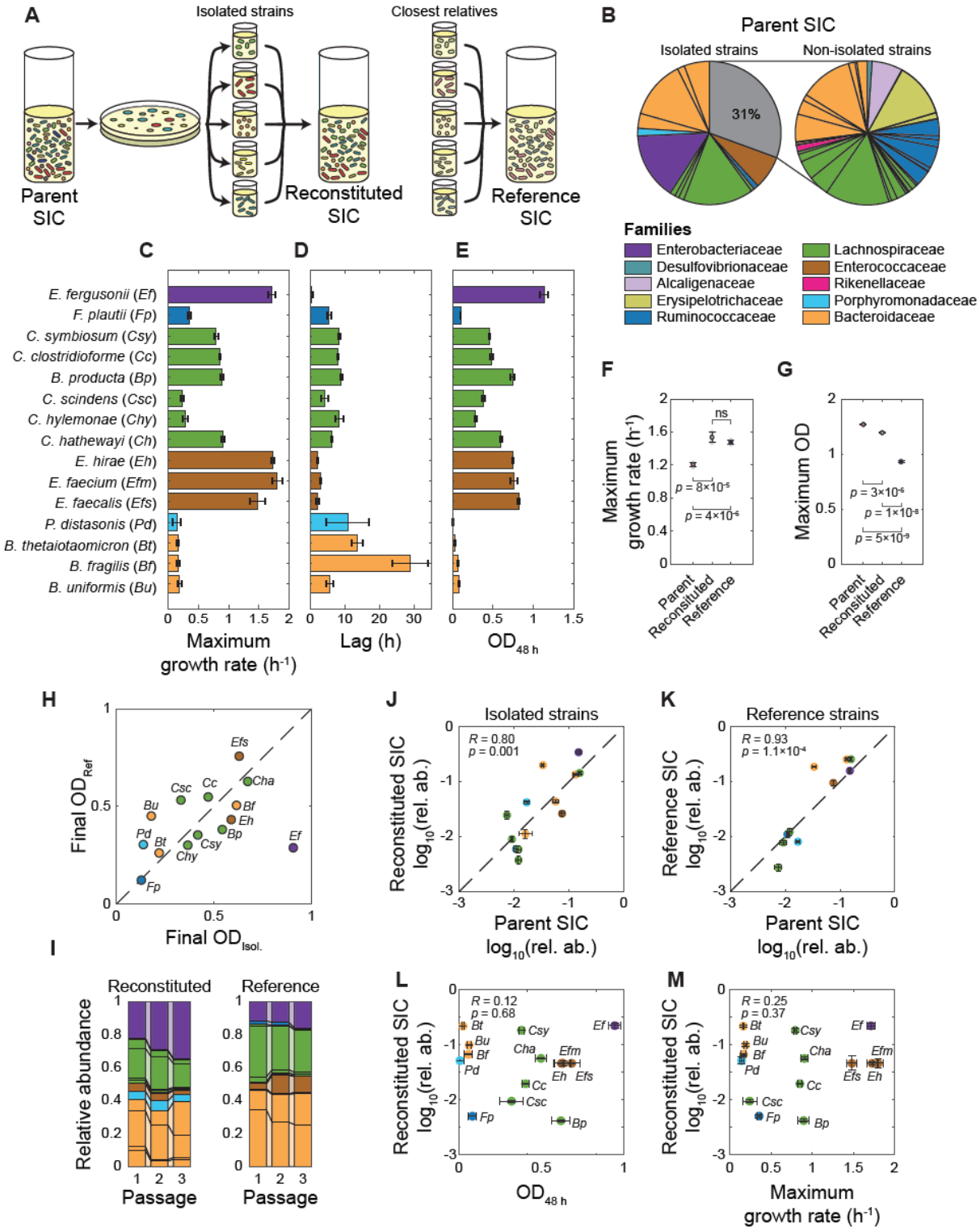

Figure 3: Community growth can be partially reconstituted from isolates.

bioRxiv preprint doi: https://doi.org/10.1101/2020.07.06.190181; this version posted July 6, 2020. The copyright holder for this preprint (which was not certified by peer review) is the author/funder. All rights reserved. No reuse allowed without permission.

A) Experimental setup. Fifteen strains representing distinct species were isolated from an SIC passaged in BHI derived from an MD mouse pre-treatment fecal sample (parent SIC). The 15 strains, or the closest relative reference strains, were mixed and co-cultured (reconstituted and reference SIC, respectively).

B) Isolated strains represent 69% of the composition of the parent SIC. Left: relative abundances of the 15 ASVs in the parent SIC. Right: normalized relative abundances of the non-isolated ASVs. Multiple strains map to a single ASV.

C-E) Isolates display a range of growth behaviors. Mean values of maximum growth rate (C), lag time (D), and OD after 48 h of growth (E) of the 15 isolates in (B). Error bars, standard deviations (SD); n=6.

F-G) Parent SIC growth characteristics are partially recapitulated by reconstituted and reference SICs. Maximum growth rate (F) and OD after 48 h of growth (G) of the parent SIC in (B), and the reconsitituted and reference SICs. Colored circles and error bars represent mean values and SD; n=4. p-values are from a Student's two-sided t-test between each pairwise comparison; ns: not significant.

H) Yields (OD after 48 h of growth in BHI) of isolates in (C-E) and corresponding reference strains are mostly correlated. Isolate abbreviations are defined in (C).

I) Relative abundances of ASVs in reconstituted (left) or reference (right) SICs during three passages in BHI. Multiple strains can be mapped to a single ASV.

bioRxiv preprint doi: https://doi.org/10.1101/2020.07.06.190181; this version posted July 6, 2020. The copyright holder for this preprint (which was not certified by peer review) is the author/funder. All rights reserved. No reuse allowed without permission.

J,K) Reconstituted (J) and reference (K) SICs converge to compositions with relative abundances similar to that of the parent SIC. Data are mean $\log_{10}$(relative abundance) of ASVs, normalized to the total relative abundance of those ASVs within the reconstituted or parent SIC. Error bars, SD; *n*=4. *R*, Pearson correlation coefficient.

L,M) Isolate growth behaviors do not correlate with their abundances in reconstituted SIC. Mean $\log_{10}$(relative abundance) of ASVs corresponding to isolates in the 3rd passage of reconstituted SIC is uncorrelated with the OD of the isolates after 48 h of growth (L) or maximum growth rate of those strains in isolation (M). Error bars, SD; *n*=4 for relative abundances, *n*=6 for OD and maximum growth rate. *R*, Pearson correlation coefficient. Where multiple strains map to a single ASV, the relative abundance of the ASV value is used for all strains that map to that ASV.

bioRxiv preprint doi: https://doi.org/10.1101/2020.07.06.190181; this version posted July 6, 2020. The copyright holder for this preprint (which was not certified by peer review) is the author/funder. All rights reserved. No reuse allowed without permission.

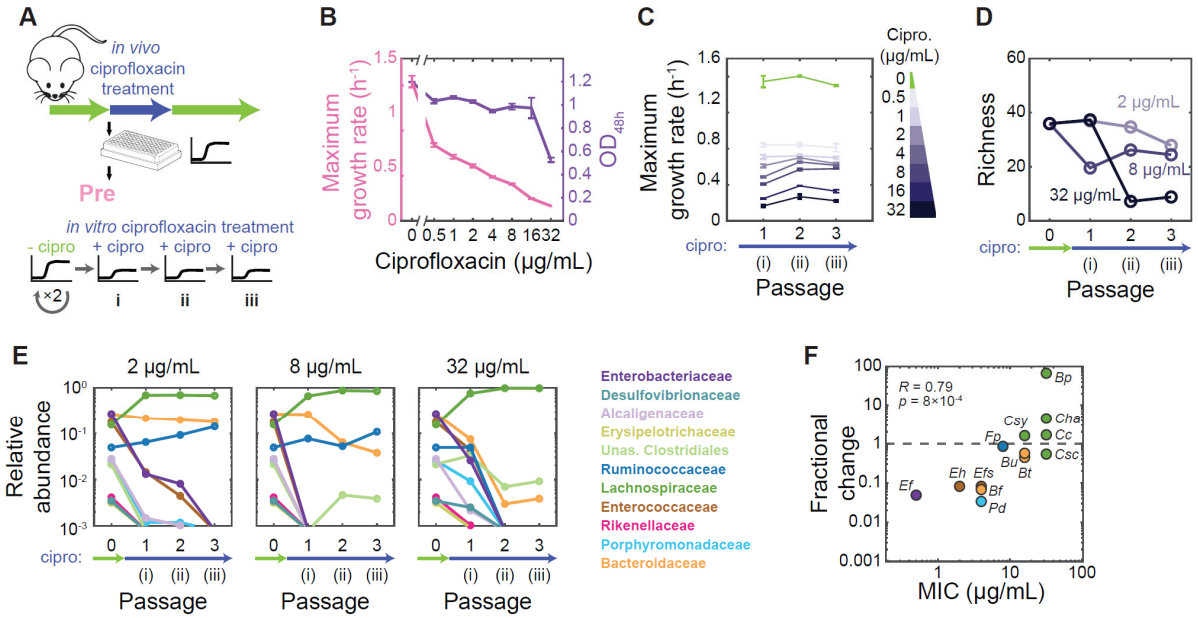

Figure 4: SIC response to ciprofloxacin can be predicted from exposure history and individual member sensitivities.

A) Experimental setup. An SIC passaged in BHI from pre-treatment humanized mouse fecal inoculum (Pre-SD) was revived after freezing and passaged twice in BHI. The SIC was then passaged in ciprofloxacin three times.

B) Pre-SD SIC yield and growth rate decrease with increasing concentrations of ciprofloxacin. OD was measured after 48 h of growth with ciprofloxacin. Lines, means of triplicate growth curves; error bars, standard deviations (SD).

C) Pre-SD SIC shows little adaptation to ciprofloxacin. Maximum growth rate decreases or remains approximately constant across three passages in ciprofloxacin. Symbols are as in (B).

bioRxiv preprint doi: https://doi.org/10.1101/2020.07.06.190181; this version posted July 6, 2020. The copyright holder for this preprint (which was not certified by peer review) is the author/funder. All rights reserved. No reuse allowed without permission.

D) Richness (number of ASVs in rarefied data) of Pre-SD SIC decreases during ciprofloxacin. Data are means of two technical replicates.

E) Ciprofloxacin treatment *in vitro* selects for a few families. Family-level composition of the Pre community across passages in ciprofloxacin. The limit of detection was estimated at 10^{-3}. Data are means of two technical replicates.

F) Growth of ASVs in the Pre-SD SIC under ciprofloxacin treatment can be predicted by their sensitivity in isolation. Fractional-abundance changes of ASVs corresponding to the 15 isolates in Fig. 3A were computed after one passage in 2 μg/mL ciprofloxacin. MICs were calculated during growth in isolation in BHI (Table S1).

bioRxiv preprint doi: https://doi.org/10.1101/2020.07.06.190181; this version posted July 6, 2020. The copyright holder for this preprint (which was not certified by peer review) is the author/funder. All rights reserved. No reuse allowed without permission.

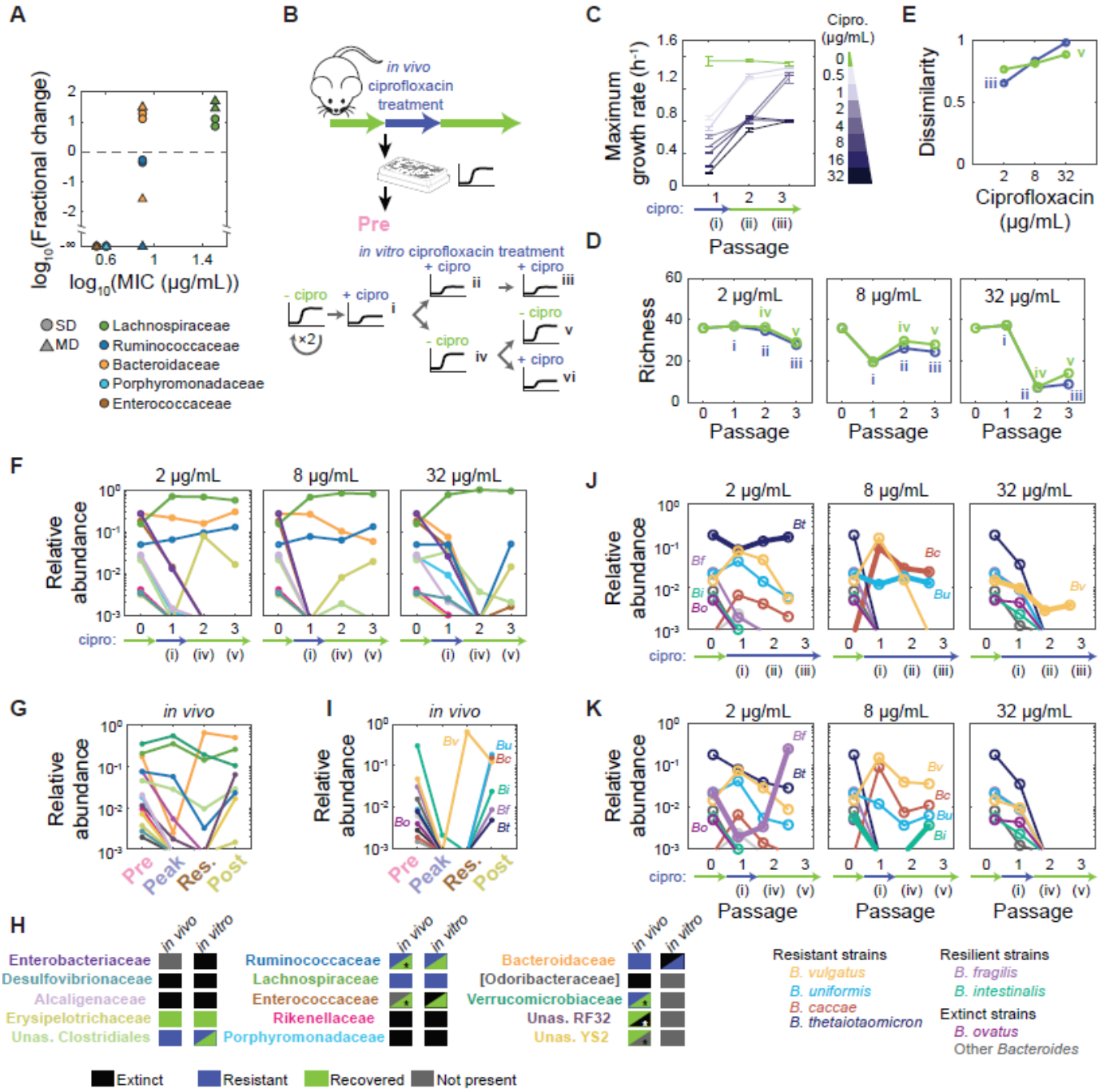

Figure 5: Ciprofloxacin treatment *in vitro* reproduces features of *in vivo* dynamics at multiple taxonomic levels.

bioRxiv preprint doi: https://doi.org/10.1101/2020.07.06.190181; this version posted July 6, 2020. The copyright holder for this preprint (which was not certified by peer review) is the author/funder. All rights reserved. No reuse allowed without permission.

A) Changes in family-level abundances during ciprofloxacin treatment *in vivo* can be predicted by strain-level sensitivities *in vitro*. Fractional changes were computed as the ratio of residual and pre-treatment time-point abundances *in vivo*. MIC is the mean value across strains in a given family determined from growth in isolation in BHI (Table S1).

B) Experimental setup mimicking *in vivo* transient treatment. An SIC passaged in BHI from pre-treatment humanized mouse fecal inoculum (Pre-SD) was revived after freezing and passaged twice in BHI. The SIC was then passaged in ciprofloxacin three times (i,ii,iii); in ciprofloxacin once and then twice without the drug (i,iv,v); or re-exposed to the drug after one round of recovery (i,iv,vi).

C) Pre-SD SIC growth rate can recover to levels similar to values before treatment at low concentrations. Maximum growth rate was calculated across ciprofloxacin concentrations during one round of antibiotic treatment and two rounds of recovery. Lines, mean of three technical replicates; error bars, standard deviations (SD).

D) Richness of Pre-SD SIC recovered only partially after removal of ciprofloxacin (green) versus continuous exposure (blue, same data as Fig. 4D). Data are the mean of two replicates.

E) The Pre-SD SIC was further remodeled after removal of low-dose antibiotic treatment. Bray-Curtis dissimilarity index of SICs was calculated after the third

bioRxiv preprint doi: https://doi.org/10.1101/2020.07.06.190181; this version posted July 6, 2020. The copyright holder for this preprint (which was not certified by peer review) is the author/funder. All rights reserved. No reuse allowed without permission.

passage in ciprofloxacin (blue) or after two rounds of recovery (green) with respect to their untreated composition. Data are the mean of two technical replicates.

F) Some families, like the Erysipelotrichaceae and Ruminococcaceae, can recover after transient ciprofloxacin treatment. Data are the mean $\log_{10}$(relative abundance) of two replicates during one round of ciprofloxacin treatment and two rounds of recovery at the family level.

G) Ciprofloxacin-induced changes to family-level abundances in SD mice *in vivo* resemble changes *in vitro* in (F). Data are the mean $\log_{10}$(relative abundance) of two mice at the family level.

H) Most families display similar qualitative abundance changes *in vivo* and *in vitro*. Split boxes denote either different responses across diets *in vivo* (asterisk denotes the response in MD mice, Fig. S9E) or across ciprofloxacin doses *in vitro*.

I) *Bacteroides* dynamics *in vivo* consist of *B. vulgatus* dominance during treatment and the recovery of several species after treatment. Data are the mean $\log_{10}$(relative abundance) of two SD mice at the ASV level: *Bacteroides ovatus* (*Bo*), *B. vulgatus* (*Bv*), *B. uniformis* (*Bu*), *B. caccae* (*Bc*), *B. intestinalis* (*Bi*), *B. fragilis* (*Bf*), and *B. thetaiotaomicron* (*Bt*). Other *Bacteroides* are shown in shades of grey.

J,K) *Bacteroides* survival and recovery *in vivo* can be respectively explained by resistance and resilience characteristics of the Pre-SD SIC *in vitro* during

bioRxiv preprint doi: https://doi.org/10.1101/2020.07.06.190181; this version posted July 6, 2020. The copyright holder for this preprint (which was not certified by peer review) is the author/funder. All rights reserved. No reuse allowed without permission.

1262 continuous treatment (J) or one round of treatment followed by two rounds of
1263 recovery (K). Data are the mean $\log_{10}$(relative abundance) of two replicates
1264 during one round of ciprofloxacin treatment and two rounds of recovery at
1265 the ASV level. Thick lines highlight *Bacteroides* ASVs that show resistance (J)
1266 or resilience (K) at the highest concentration that they display the behavior.

bioRxiv preprint doi: https://doi.org/10.1101/2020.07.06.190181; this version posted July 6, 2020. The copyright holder for this preprint (which was not certified by peer review) is the author/funder. All rights reserved. No reuse allowed without permission.

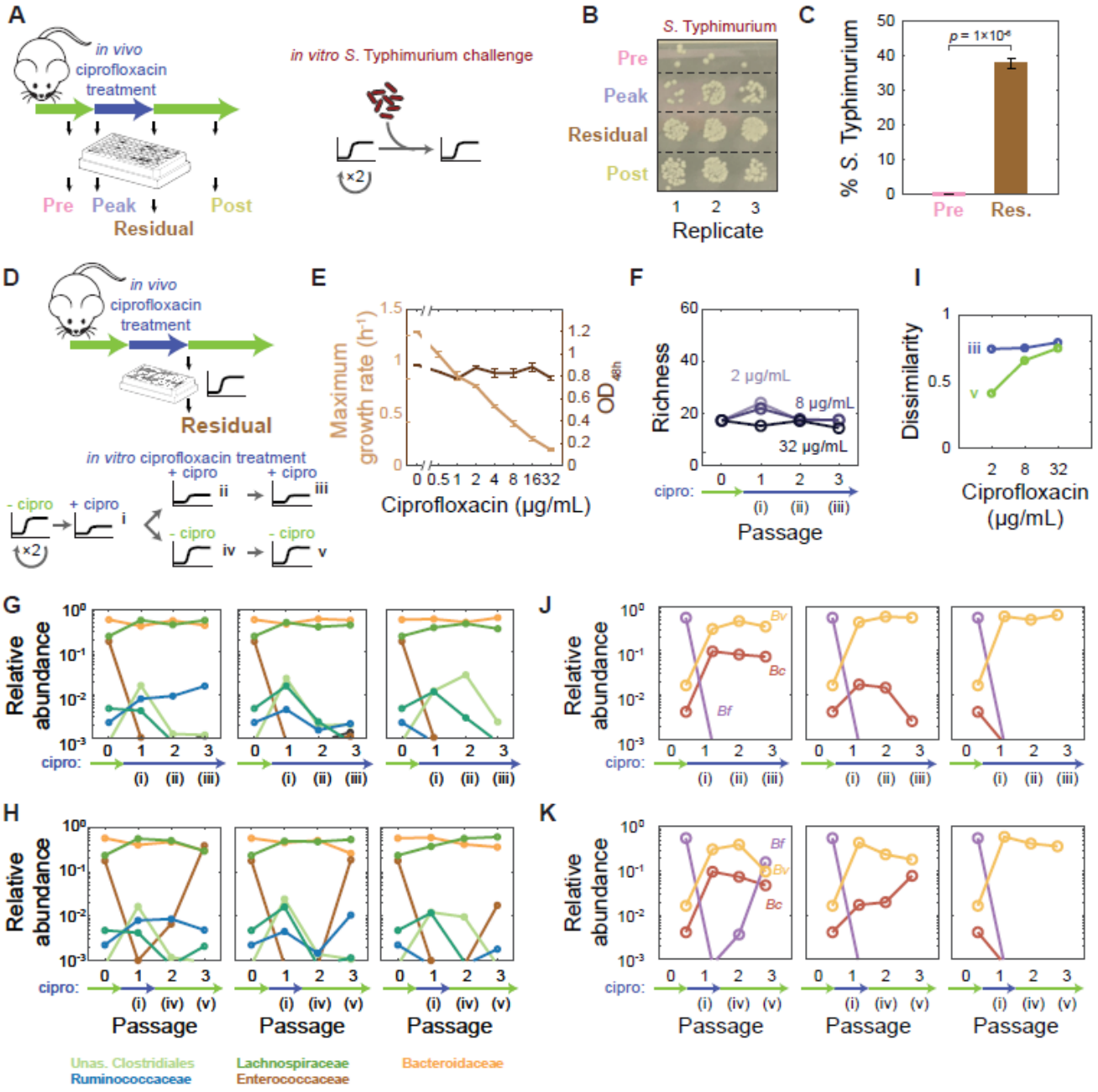

Figure 6: Pre-exposure of the gut microbiota to ciprofloxacin *in vivo* results in functional differences *in vitro*.

A) Experimental setup for *in vitro* challenge with *S.* Typhimurium. SICs passaged in BHI from pre-, peak, residual, and post-treatment humanized mouse fecal

bioRxiv preprint doi: https://doi.org/10.1101/2020.07.06.190181; this version posted July 6, 2020. The copyright holder for this preprint (which was not certified by peer review) is the author/funder. All rights reserved. No reuse allowed without permission.

inocula were revived after freezing and passaged twice in BHI. SICs were mixed with *S*. Typhimurium and *S*. Typhimurium levels were quantified after 48 h of growth.

B) SICs derived from mice treated with ciprofloxacin are more susceptible to *S*. Typhimurium. Colonies of *S*. Typhimurium SL1344 after 48 h of growth with SICs diluted $1{:}10^4$ and grown aerobically on LB+streptomycin.

C) Single-cell quantification of mCherry-tagged *S*. Typhimurium 14028s after co-culture with SICs derived from pre- and residual-treatment mice fecal inocula. *p*-value is from a Student's two-sided *t*-test; n=3.

D) Experimental setup for *in vitro* antibiotic treatment of a pre-exposed SIC. An SIC passaged in BHI from residual treatment humanized mouse fecal inoculum (Res-SD) was revived after freezing and passaged twice in BHI. The SIC was passaged in ciprofloxacin three times (i,ii,iii) or in ciprofloxacin once and then twice without the drug (i,iv,v).

E) In contrast to the Pre-SD SIC (Fig. 4B), the yield and of Res-SD SIC is virtually unaffected by ciprofloxacin, although the growth rate decreases with concentration. OD was measured after 48 h of growth with ciprofloxacin. Lines, means of triplicate growth curves; error bars, standard deviations (SD).

bioRxiv preprint doi: https://doi.org/10.1101/2020.07.06.190181; this version posted July 6, 2020. The copyright holder for this preprint (which was not certified by peer review) is the author/funder. All rights reserved. No reuse allowed without permission.

F) Richness (number of ASVs in rarefied data) of Pre-SD SIC remains constant during continuous ciprofloxacin treatment. Data are means of two technical replicates.

G) Bacteroidaceae and Lachnospiraceae dominate during three rounds of ciprofloxacin treatment of the Res-SD SIC. Data are the mean of family-level abundances across two technical replicates.

H) Enterococcaceae can recover after one round of ciprofloxacin treatment in the Res-SD SIC. Data are the mean of two replicates.

I) Res-SD SIC diversity can recover after ciprofloxacin removal. The Bray-Curtis dissimilarity index of SICs at the third passage in ciprofloxacin (blue) or after two rounds of recovery (green), compared to their untreated compositions. Data are the mean of two replicates.

G,H) Bacteroidaceae are remodeled in the Res-SD SIC during and after ciprofloxacin treatment, with *B. vulgatus* as the only member to generally survive. Relative abundances of *Bacteroides* species in the Res-SD SIC during continuous ciprofloxacin treatment (G) or after one round of treatment followed by two rounds of recovery (H).

bioRxiv preprint doi: https://doi.org/10.1101/2020.07.06.190181; this version posted July 6, 2020. The copyright holder for this preprint (which was not certified by peer review) is the author/funder. All rights reserved. No reuse allowed without permission.

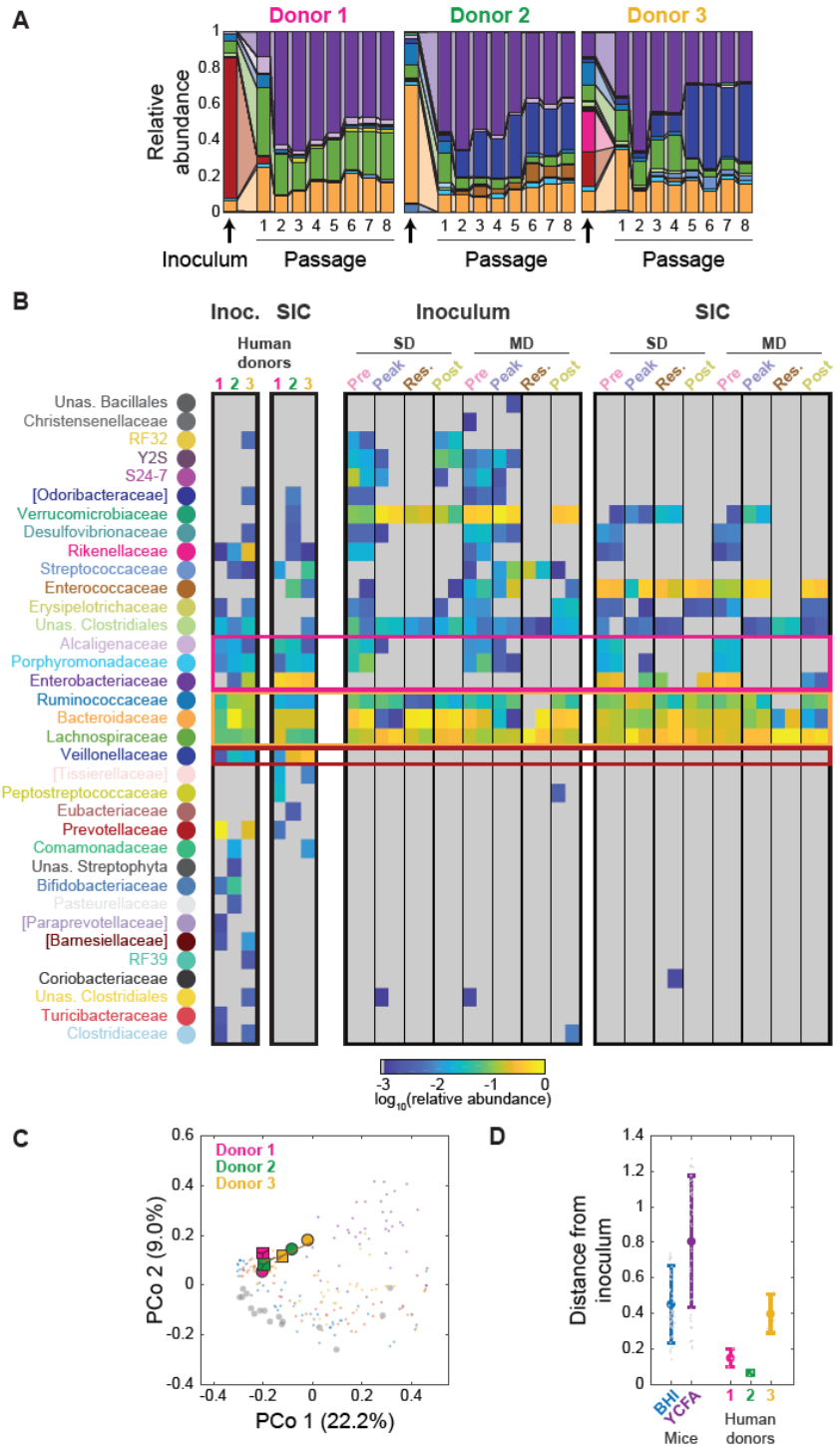

1307

1308 **Figure 7: Batch culturing of human stool leads to stable and complex SICs.**

bioRxiv preprint doi: https://doi.org/10.1101/2020.07.06.190181; this version posted July 6, 2020. The copyright holder for this preprint (which was not certified by peer review) is the author/funder. All rights reserved. No reuse allowed without permission.

A) *In vitro* passaging of stool samples from three healthy human donors in BHI produced stable, complex SICs. Family-level composition; each passage was 48 h. Colors corresponding to individual families are as in (B).

B) *In vitro* passaging of stool samples leads to SICs that maintain many families from the fecal microbiota. Mean relative abundance of three technical replicates for each inoculum and corresponding 7th passage SIC in (A) (left) and all humanized mice SICs (right). Only families with mean relative abundance >0.1% are shown; undetectable taxa are shown in grey. Boxes highlight families common to all SICs (orange), present in all human donor SICs but underrepresented in humanized mice SICs (pink), and exclusive to all human donor SICs (red).

C) Passaging in BHI preserves the beta diversity of human stool inocula. PCoA was computed with unweighted Unifrac distances using all 192 passaged SICs inoculated with humanized mouse samples in Fig. 2A and the SICs in (A). Colors and shapes are as in (C). Symbols represent the centroid of three replicates; lines connect replicates to the centroid. SICs from humanized mice are shown in colors in smaller dots in the same colors as in Fig. 1G and the humanized mice fecal samples are shown in gray.

D) Human stool-derived SICs are as similar to their inocula as humanized mice-derived SICs, based on weighted Unifrac distances between steady-state SICs

bioRxiv preprint doi: https://doi.org/10.1101/2020.07.06.190181; this version posted July 6, 2020. The copyright holder for this preprint (which was not certified by peer review) is the author/funder. All rights reserved. No reuse allowed without permission.

and their fecal inocula. SICs derived from humanized mice passaged in BHI or YCFA are shown for comparison (data from Fig. 2B). Colored circles are the mean of SICs (n=48 for BHI and YCFA humanized mouse SICs and n=3 for BHI human donor SICs). Error bars, standard deviations. Individual data points are shown in gray.

bioRxiv preprint doi: https://doi.org/10.1101/2020.07.06.190181; this version posted July 6, 2020. The copyright holder for this preprint (which was not certified by peer review) is the author/funder. All rights reserved. No reuse allowed without permission.

References

Adamowicz, E.M., Flynn, J., Hunter, R.C., and Harcombe, W.R. (2018). Cross-feeding modulates antibiotic tolerance in bacterial communities. ISME J.

Aranda-Díaz, A., Obadia, B., Thomsen, T., Hallberg, Z.F., Güvener, Z.T., Ludington, W.B., and Huang, K.C. (2019). Bacterial interspecies interactions modulate pH-mediated antibiotic tolerance in a model gut microbiota. BioRxiv.

Auchtung, J.M., Robinson, C.D., Farrell, K., and Britton, R.A. (2016). MiniBioReactor Arrays (MBRAs) as a Tool for Studying C. difficile Physiology in the Presence of a Complex Community. Methods Mol Biol *1476*, 235-258.

Baev, M.V., Baev, D., Radek, A.J., and Campbell, J.W. (2006). Growth of Escherichia coli MG1655 on LB medium: determining metabolic strategy with transcriptional microarrays. Appl Microbiol Biotechnol *71*, 323-328.

Barroso-Batista, J., Pedro, M.F., Sales-Dias, J., Pinto, C.J.G., Thompson, J.A., Pereira, H., Demengeot, J., Gordo, I., and Xavier, K.B. (2020). Specific Eco-evolutionary Contexts in the Mouse Gut Reveal Escherichia coli Metabolic Versatility. Curr Biol *30*, 1049-1062 e1047.

Barthel, M., Hapfelmeier, S., Quintanilla-Martinez, L., Kremer, M., Rohde, M., Hogardt, M., Pfeffer, K., Russmann, H., and Hardt, W.D. (2003). Pretreatment of mice with

bioRxiv preprint doi: https://doi.org/10.1101/2020.07.06.190181; this version posted July 6, 2020. The copyright holder for this preprint (which was not certified by peer review) is the author/funder. All rights reserved. No reuse allowed without permission.

1353 streptomycin provides a Salmonella enterica serovar Typhimurium colitis model that
1354 allows analysis of both pathogen and host. Infect Immun *71*, 2839-2858.
1355 Becker, N., Kunath, J., Loh, G., and Blaut, M. (2011). Human intestinal microbiota:
1356 characterization of a simplified and stable gnotobiotic rat model. Gut Microbes *2*, 25-33.
1357 Browne, H.P., Forster, S.C., Anonye, B.O., Kumar, N., Neville, B.A., Stares, M.D.,
1358 Goulding, D., and Lawley, T.D. (2016). Culturing of 'unculturable' human microbiota
1359 reveals novel taxa and extensive sporulation. Nature *533*, 543-546.
1360 Callahan, B.J., McMurdie, P.J., Rosen, M.J., Han, A.W., Johnson, A.J., and Holmes, S.P.
1361 (2016). DADA2: High-resolution sample inference from Illumina amplicon data. Nat
1362 Methods *13*, 581-583.
1363 Cammarota, G., Ianiro, G., Tilg, H., Rajilic-Stojanovic, M., Kump, P., Satokari, R., Sokol,
1364 H., Arkkila, P., Pintus, C., Hart, A., *et al.* (2017). European consensus conference on
1365 faecal microbiota transplantation in clinical practice. Gut *66*, 569-580.
1366 Caporaso, J.G., Kuczynski, J., Stombaugh, J., Bittinger, K., Bushman, F.D., Costello, E.K.,
1367 Fierer, N., Pena, A.G., Goodrich, J.K., Gordon, J.I., *et al.* (2010). QIIME allows analysis of
1368 high-throughput community sequencing data. Nat Methods *7*, 335-336.
1369 Carman, R.J., Simon, M.A., Fernandez, H., Miller, M.A., and Bartholomew, M.J. (2004).
1370 Ciprofloxacin at low levels disrupts colonization resistance of human fecal microflora
1371 growing in chemostats. Regul Toxicol Pharmacol *40*, 319-326.

bioRxiv preprint doi: https://doi.org/10.1101/2020.07.06.190181; this version posted July 6, 2020. The copyright holder for this preprint (which was not certified by peer review) is the author/funder. All rights reserved. No reuse allowed without permission.

1372 Cho, I., Yamanishi, S., Cox, L., Methe, B.A., Zavadil, J., Li, K., Gao, Z., Mahana, D., Raju,
1373 K., Teitler, I., *et al.* (2012). Antibiotics in early life alter the murine colonic microbiome
1374 and adiposity. Nature *488*, 621-626.
1375 Cox, L.M., Yamanishi, S., Sohn, J., Alekseyenko, A.V., Leung, J.M., Cho, I., Kim, S.G., Li,
1376 H., Gao, Z., Mahana, D., *et al.* (2014). Altering the intestinal microbiota during a critical
1377 developmental window has lasting metabolic consequences. Cell *158*, 705-721.
1378 de Vos, M.G.J., Zagorski, M., McNally, A., and Bollenbach, T. (2017). Interaction
1379 networks, ecological stability, and collective antibiotic tolerance in polymicrobial
1380 infections. Proc Natl Acad Sci U S A *114*, 10666-10671.
1381 Del Monte-Luna, P., Brook, B.W., Zetina-Rejón, M.J., and Cruz-Escalona, V.H. (2004).
1382 The carrying capacity of ecosystems. Global Ecology and Biogeography *13*, 485-495.
1383 Dethlefsen, L., and Relman, D.A. (2011). Incomplete recovery and individualized
1384 responses of the human distal gut microbiota to repeated antibiotic perturbation. Proc
1385 Natl Acad Sci U S A *108 Suppl 1*, 4554-4561.
1386 Doorduyn, Y., Van Den Brandhof, W.E., Van Duynhoven, Y.T., Wannet, W.J., and Van
1387 Pelt, W. (2006). Risk factors for Salmonella Enteritidis and Typhimurium (DT104 and
1388 non-DT104) infections in The Netherlands: predominant roles for raw eggs in
1389 Enteritidis and sandboxes in Typhimurium infections. Epidemiol Infect *134*, 617-626.

bioRxiv preprint doi: https://doi.org/10.1101/2020.07.06.190181; this version posted July 6, 2020. The copyright holder for this preprint (which was not certified by peer review) is the author/funder. All rights reserved. No reuse allowed without permission.

1390 Drekonja, D., Reich, J., Gezahegn, S., Greer, N., Shaukat, A., MacDonald, R., Rutks, I.,
1391 and Wilt, T.J. (2015). Fecal Microbiota Transplantation for Clostridium difficile
1392 Infection: A Systematic Review. Ann Intern Med *162*, 630-638.
1393 Faith, J.J., McNulty, N.P., Rey, F.E., and Gordon, J.I. (2011). Predicting a human gut
1394 microbiota's response to diet in gnotobiotic mice. Science *333*, 101-104.
1395 Frohlich, E.E., Farzi, A., Mayerhofer, R., Reichmann, F., Jacan, A., Wagner, B., Zinser, E.,
1396 Bordag, N., Magnes, C., Frohlich, E., *et al.* (2016). Cognitive impairment by antibiotic-
1397 induced gut dysbiosis: Analysis of gut microbiota-brain communication. Brain Behav
1398 Immun *56*, 140-155.
1399 Goldford, J.E., Lu, N., Bajic, D., Estrela, S., Tikhonov, M., Sanchez-Gorostiaga, A., Segre,
1400 D., Mehta, P., and Sanchez, A. (2018). Emergent simplicity in microbial community
1401 assembly. Science *361*, 469-474.
1402 Gutierrez, N., and Garrido, D. (2019). Species Deletions from Microbiome Consortia
1403 Reveal Key Metabolic Interactions between Gut Microbes. mSystems *4*.
1404 Hooper, L.V., Littman, D.R., and Macpherson, A.J. (2012). Interactions between the
1405 microbiota and the immune system. Science *336*, 1268-1273.
1406 Hwang, I., Park, Y.J., Kim, Y.R., Kim, Y.N., Ka, S., Lee, H.Y., Seong, J.K., Seok, Y.J., and
1407 Kim, J.B. (2015). Alteration of gut microbiota by vancomycin and bacitracin improves
1408 insulin resistance via glucagon-like peptide 1 in diet-induced obesity. FASEB J *29*, 2397-
1409 2411.

bioRxiv preprint doi: https://doi.org/10.1101/2020.07.06.190181; this version posted July 6, 2020. The copyright holder for this preprint (which was not certified by peer review) is the author/funder. All rights reserved. No reuse allowed without permission.

Ivanov, II, Frutos Rde, L., Manel, N., Yoshinaga, K., Rifkin, D.B., Sartor, R.B., Finlay, B.B., and Littman, D.R. (2008). Specific microbiota direct the differentiation of IL-17-producing T-helper cells in the mucosa of the small intestine. Cell Host Microbe *4*, 337-349.

Johansson, M.E., Jakobsson, H.E., Holmen-Larsson, J., Schutte, A., Ermund, A., Rodriguez-Pineiro, A.M., Arike, L., Wising, C., Svensson, F., Backhed, F., *et al.* (2015). Normalization of Host Intestinal Mucus Layers Requires Long-Term Microbial Colonization. Cell Host Microbe *18*, 582-592.

Kashyap, P.C., Marcobal, A., Ursell, L.K., Larauche, M., Duboc, H., Earle, K.A., Sonnenburg, E.D., Ferreyra, J.A., Higginbottom, S.K., Million, M., *et al.* (2013). Complex interactions among diet, gastrointestinal transit, and gut microbiota in humanized mice. Gastroenterology *144*, 967-977.

Kehe, J., Kulesa, A., Ortiz, A., Ackerman, C.M., Thakku, S.G., Sellers, D., Kuehn, S., Gore, J., Friedman, J., and Blainey, P.C. (2019). Massively parallel screening of synthetic microbial communities. Proc Natl Acad Sci U S A *116*, 12804-12809.

Khoruts, A., and Weingarden, A.R. (2014). Emergence of fecal microbiota transplantation as an approach to repair disrupted microbial gut ecology. Immunol Lett *162*, 77-81.

bioRxiv preprint doi: https://doi.org/10.1101/2020.07.06.190181; this version posted July 6, 2020. The copyright holder for this preprint (which was not certified by peer review) is the author/funder. All rights reserved. No reuse allowed without permission.

1428 Lawley, T.D., Bouley, D.M., Hoy, Y.E., Gerke, C., Relman, D.A., and Monack, D.M.
1429 (2008). Host transmission of Salmonella enterica serovar Typhimurium is controlled by
1430 virulence factors and indigenous intestinal microbiota. Infect Immun *76*, 403-416.
1431 Le Bastard, Q., Ward, T., Sidiropoulos, D., Hillmann, B.M., Chun, C.L., Sadowsky, M.J.,
1432 Knights, D., and Montassier, E. (2018). Fecal microbiota transplantation reverses
1433 antibiotic and chemotherapy-induced gut dysbiosis in mice. Sci Rep *8*, 6219.
1434 Lozupone, C., and Knight, R. (2005). UniFrac: a new phylogenetic method for
1435 comparing microbial communities. Appl Environ Microbiol *71*, 8228-8235.
1436 Lozupone, C.A., Hamady, M., Kelley, S.T., and Knight, R. (2007). Quantitative and
1437 qualitative beta diversity measures lead to different insights into factors that structure
1438 microbial communities. Appl Environ Microbiol *73*, 1576-1585.
1439 Macfarlane, G.T., Macfarlane, S., and Gibson, G.R. (1998). Validation of a Three-Stage
1440 Compound Continuous Culture System for Investigating the Effect of Retention Time
1441 on the Ecology and Metabolism of Bacteria in the Human Colon. Microb Ecol *35*, 180-
1442 187.
1443 Mark Welch, J.L., Hasegawa, Y., McNulty, N.P., Gordon, J.I., and Borisy, G.G. (2017).
1444 Spatial organization of a model 15-member human gut microbiota established in
1445 gnotobiotic mice. Proc Natl Acad Sci U S A *114*, E9105-E9114.
1446 Mayer, E.A., Knight, R., Mazmanian, S.K., Cryan, J.F., and Tillisch, K. (2014). Gut
1447 microbes and the brain: paradigm shift in neuroscience. J Neurosci *34*, 15490-15496.

bioRxiv preprint doi: https://doi.org/10.1101/2020.07.06.190181; this version posted July 6, 2020. The copyright holder for this preprint (which was not certified by peer review) is the author/funder. All rights reserved. No reuse allowed without permission.

1448 Minekus, M., Smeets-Peeters, M., Bernalier, A., Marol-Bonnin, S., Havenaar, R.,
1449 Marteau, P., Alric, M., Fonty, G., and Huis in't Veld, J.H. (1999). A computer-controlled
1450 system to simulate conditions of the large intestine with peristaltic mixing, water
1451 absorption and absorption of fermentation products. Appl Microbiol Biotechnol *53*, 108-
1452 114.
1453 Ng, K.M., Aranda-Diaz, A., Tropini, C., Frankel, M.R., Van Treuren, W.W., O'Laughlin,
1454 C., Merrill, B.D., Yu, F.B., Pruss, K.M., Oliveira, R.A., *et al.* (2019). Recovery of the gut
1455 microbiota after antibiotics depends on host diet and environmental reservoirs. Cell
1456 Host Microbe.
1457 Ng, K.M., Ferreyra, J.A., Higginbottom, S.K., Lynch, J.B., Kashyap, P.C., Gopinath, S.,
1458 Naidu, N., Choudhury, B., Weimer, B.C., Monack, D.M., *et al.* (2013). Microbiota-
1459 liberated host sugars facilitate post-antibiotic expansion of enteric pathogens. Nature
1460 *502*, 96-99.
1461 Nicoloff, H., and Andersson, D.I. (2016). Indirect resistance to several classes of
1462 antibiotics in cocultures with resistant bacteria expressing antibiotic-modifying or -
1463 degrading enzymes. J Antimicrob Chemother *71*, 100-110.
1464 Pavia, A.T., Shipman, L.D., Wells, J.G., Puhr, N.D., Smith, J.D., McKinley, T.W., and
1465 Tauxe, R.V. (1990). Epidemiologic evidence that prior antimicrobial exposure decreases
1466 resistance to infection by antimicrobial-sensitive Salmonella. J Infect Dis *161*, 255-260.

bioRxiv preprint doi: https://doi.org/10.1101/2020.07.06.190181; this version posted July 6, 2020. The copyright holder for this preprint (which was not certified by peer review) is the author/funder. All rights reserved. No reuse allowed without permission.

1467 Rettedal, E.A., Gumpert, H., and Sommer, M.O. (2014). Cultivation-based multiplex
1468 phenotyping of human gut microbiota allows targeted recovery of previously
1469 uncultured bacteria. Nat Commun *5*, 4714.
1470 Reyes, A., Wu, M., McNulty, N.P., Rohwer, F.L., and Gordon, J.I. (2013). Gnotobiotic
1471 mouse model of phage-bacterial host dynamics in the human gut. Proc Natl Acad Sci U
1472 S A *110*, 20236-20241.
1473 Rezzonico, E., Mestdagh, R., Delley, M., Combremont, S., Dumas, M.E., Holmes, E.,
1474 Nicholson, J., and Bibiloni, R. (2011). Bacterial adaptation to the gut environment favors
1475 successful colonization: microbial and metabonomic characterization of a simplified
1476 microbiota mouse model. Gut Microbes *2*, 307-318.
1477 Sanchez-Vizuete, P., Orgaz, B., Aymerich, S., Le Coq, D., and Briandet, R. (2015).
1478 Pathogens protection against the action of disinfectants in multispecies biofilms. Front
1479 Microbiol *6*, 705.
1480 Schubert, A.M., Sinani, H., and Schloss, P.D. (2015). Antibiotic-Induced Alterations of
1481 the Murine Gut Microbiota and Subsequent Effects on Colonization Resistance against
1482 Clostridium difficile. MBio *6*, e00974.
1483 Shi, H., Colavin, A., Lee, T.K., and Huang, K.C. (2017). Strain Library Imaging Protocol
1484 for high-throughput, automated single-cell microscopy of large bacterial collections
1485 arrayed on multiwell plates. Nat Protoc *12*, 429-438.

bioRxiv preprint doi: https://doi.org/10.1101/2020.07.06.190181; this version posted July 6, 2020. The copyright holder for this preprint (which was not certified by peer review) is the author/funder. All rights reserved. No reuse allowed without permission.

1486 Sonnenburg, E.D., Smits, S.A., Tikhonov, M., Higginbottom, S.K., Wingreen, N.S., and
1487 Sonnenburg, J.L. (2016). Diet-induced extinctions in the gut microbiota compound over
1488 generations. Nature *529*, 212-215.
1489 Sonnenburg, J.L., and Backhed, F. (2016). Diet-microbiota interactions as moderators of
1490 human metabolism. Nature *535*, 56-64.
1491 Stecher, B., Robbiani, R., Walker, A.W., Westendorf, A.M., Barthel, M., Kremer, M.,
1492 Chaffron, S., Macpherson, A.J., Buer, J., Parkhill, J., *et al.* (2007). Salmonella enterica
1493 serovar typhimurium exploits inflammation to compete with the intestinal microbiota.
1494 PLoS Biol *5*, 2177-2189.
1495 Tramontano, M., Andrejev, S., Pruteanu, M., Klunemann, M., Kuhn, M., Galardini, M.,
1496 Jouhten, P., Zelezniak, A., Zeller, G., Bork, P., *et al.* (2018). Nutritional preferences of
1497 human gut bacteria reveal their metabolic idiosyncrasies. Nat Microbiol *3*, 514-522.
1498 Tropini, C., Moss, E.L., Merrill, B.D., Ng, K.M., Higginbottom, S.K., Casavant, E.P.,
1499 Gonzalez, C.G., Fremin, B., Bouley, D.M., Elias, J.E., *et al.* (2018). Transient Osmotic
1500 Perturbation Causes Long-Term Alteration to the Gut Microbiota. Cell *173*, 1742-1754
1501 e1717.
1502 Turnbaugh, P.J., Ridaura, V.K., Faith, J.J., Rey, F.E., Knight, R., and Gordon, J.I. (2009).
1503 The effect of diet on the human gut microbiome: a metagenomic analysis in humanized
1504 gnotobiotic mice. Sci Transl Med *1*, 6ra14.

bioRxiv preprint doi: https://doi.org/10.1101/2020.07.06.190181; this version posted July 6, 2020. The copyright holder for this preprint (which was not certified by peer review) is the author/funder. All rights reserved. No reuse allowed without permission.

1505 Van de Wiele, T., Van den Abbeele, P., Ossieur, W., Possemiers, S., and Marzorati, M.
1506 (2015). The Simulator of the Human Intestinal Microbial Ecosystem (SHIME((R))). In
1507 The Impact of Food Bioactives on Health: in vitro and ex vivo models, K. Verhoeckx, P.
1508 Cotter, I. Lopez-Exposito, C. Kleiveland, T. Lea, A. Mackie, T. Requena, D. Swiatecka,
1509 and H. Wichers, eds. (Cham (CH)), pp. 305-317.
1510 Venturelli, O.S., Carr, A.C., Fisher, G., Hsu, R.H., Lau, R., Bowen, B.P., Hromada, S.,
1511 Northen, T., and Arkin, A.P. (2018). Deciphering microbial interactions in synthetic
1512 human gut microbiome communities. Mol Syst Biol *14*, e8157.
1513 Zimmermann, M., Zimmermann-Kogadeeva, M., Wegmann, R., and Goodman, A.L.
1514 (2019). Separating host and microbiome contributions to drug pharmacokinetics and
1515 toxicity. Science *363*.
1516